

國立交通大學
顯示科技研究所
碩士論文

單載波調變與多天線輸入多天線輸出傳輸
技術應用於 60 GHz 光載微波無線訊號系統

Multiple-Input Multiple-Output Technology in
60 GHz Radio-over-Fiber System with
Single Carrier Modulation

研究生：李維元
指導教授：陳智弘 教授

中華民國一百年九月

Multiple-Input Multiple-Output Technology in 60 GHz Radio-over-Fiber System with Single Carrier Modulation

研究生: 李維元

Student: Wei-Yuan Lee

指導教授: 陳智弘

advisor: Jye-Hong Chen



Thesis submitted to the Display Institute
College of Electrical Engineering and Computer Science
National Chiao Tung University
in partial fulfillment of the requirements
for the degree of Master in Display Institute
September 2011

Acknowledgments

時光匆匆，一眨眼，兩年的碩士班生涯已經接近尾聲，這一路走來沒有特別的驚濤駭浪，沒有大起大落的電影情節，一路走得十分踏實，按部就班的完成每一個目標，能走的這麼順利，需要感謝的人實在是太多了，首先感謝我的指導教授 陳智弘老師，不僅提供完善的學習環境和實驗設備，也讓我學習到許多待人處事原則，更使我對於 ” 學習 ” 這兩個字有更深刻的體悟。由衷的感謝 林俊廷老師總在我學習的路上提點一盞明燈，和老師的討論之中也學習到非常多研究的方法與對實驗的態度，使得論文能順利完成。另外，也非常感謝 魏嘉建老師在我研究所生涯中對我的幫助。

特別的感謝 施伯宗學長、江文智學長以及陳星宇學長在實驗上以及程式上對我的幫助，不厭其煩的指導與幫忙讓我節省了許多摸索的時間。再來還要感謝實驗室的同學們 宜旻、冠穎、上詠、明義及俊鴻，與他們的相處，讓碩班生活更加豐富與充實。也十分感謝學弟妹 致勻、宗紘、威爾、勁威、頊宸、信豪、志傑、厚茨與乃慧等人的幫忙。也謝謝所有曾經幫助過我的人，謝謝你們。

最後要謝謝我的父母與家人，能給我一個衣食無缺的環境，讓我能全心全意的完成碩士學業，你們的支持是我前進的動力。

另一段旅程即將展開，但是我永遠也不會忘記我在交大所經歷過、感受過、學習過的一切，謝謝你 交大! 再會了 交大!

多天線輸入多天線輸出傳輸技術應用於 60 GHz 光載微波無線訊號系統

學生：李維元

指導教授：陳智弘 教授

國立交通大學 顯示科技研究所 碩士班

摘要

互動式多媒體的快速發展，導致新的無線網路服務不斷推陳出新，對於傳輸速度的要求也逐漸升高，帶動了 multi-Gbps 無線傳輸技術的發展。然而，60 GHz 的免授權頻段其頻寬限制在 7 GHz，並且 60 GHz 的微波訊號在空氣中有著非常大的衰減，較適合短距離的無線傳輸。因此，60 GHz 的光載微波無線訊號系統搭配上空間多工的 MIMO 技術是一個非常可實現的一個方法，提供一個寬頻、覆蓋範圍廣以及機動性兼具的服務。

在此篇論文中，藉由頻域等化器實現 2 x 2 MIMO 技術，提高頻譜使用效率達成傳輸資料倍增的效果。我們在實驗上成功傳輸 60GHz 頻段上 7 GHz 免授權頻寬的 16-QAM MIMO 單載波訊號，傳輸速度達到 2 x 13.575 Gb/s，在經過 25 公里的單模光纖和 3 公尺的無線傳輸以後，訊號品質幾乎沒有改變。

60 GHz Radio-over-Fiber System with Multiple-Input Multiple-Output Technology

Student: Wei-Yuan Lee

Advisor: Dr. Jye-Hong Chen

Display Institute, National Chiao Tung University

Abstract

The rapid growth of data rates of new wireless applications led by interactive multimedia services is driving the need for multi-Gbps wireless communication technologies in the near future. However, the bandwidth of the license free spectrum at 60 GHz is limit to 7 GHz and 60-GHz millimeter-waves have very high propagation losses rendering them more suitable for short-range wireless links ($\sim 10\text{m}$). Therefore, 60-GHz radio-over-fiber (RoF) system with spatial-multiplexing MIMO technology is a promising candidate to provide broadband service, wide coverage, and mobility.

In this these, 2×2 MIMO technique is realized by frequency domain equalizer (FDE) to improve spectrum efficiency doubling the data throughput. We experimentally demonstrate 2×13.575 Gb/s 16-QAM MIMO single carrier signal transmission within 7-GHz license-free bandwidth at 60-GHz band. The power penalty is negligible after transmission over 25-km single mode fiber and 3m wireless distance.

CONTENTS

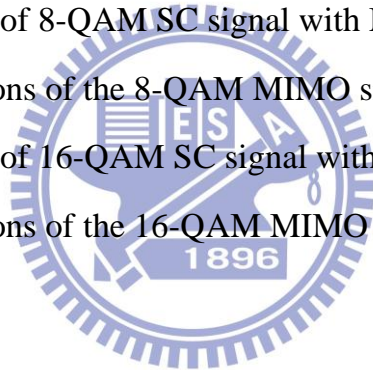
Acknowledgements.....	ii
Chinese Abstract	iii
English Abstract.....	iv
Contents	v
List of Figure	vii
Chapter 1 Introduction.....	1
1.1 Background	1
1.2 Motivation	2
1.3 Objection and Problem Statement	4
Chapter 2 Multiple-Input Multiple-output Technology.....	5
2.1 Preface	5
2.2 MIMO Technology for Improving Performance	6
2.2.1 Diversity	6
2.2.2 Alamouti Space-Time Code.....	7
2.3 MIMO Technology for Improving Capacity	10
2.3.1 Spatial Multiplexing : Zero-Forcing Receiver	12
2.3.2 Spatial Multiplexing : Maximum-Likelihood Receiver.....	16
Chapter 3 Single Carrier Frequency Domain Equalizer	18
3.1 Preface	18
3.2 Inter-Symbol Interference	18
3.3 Linear Convolution and Circular Convolution	19
3.4 Single Carrier Frequency Domain Equalizer	20
3.5 MIMO Technology with Frequency Domain Equalizer	22
Chapter 4 The Theoretical Calculation of Proposed System.....	25
4.1 Introduction Mach-Zehnder Modulator	25

4.2	Theoretical calculation of single drive MZM.....	28
4.2.1	Bias at Maximum Transmission Point	28
4.2.2	Bias at Quadrature Point	30
4.2.3	Bias at Null Point.....	30
4.3	The Concept of The Proposed System	31
4.4	Theoretical Calculation of The Proposed System.....	32
Chapter 5	Experimental Demonstration of The Proposed System	35
5.1	Preface	35
5.2	Experiment Setup	35
5.3	Experimental Result for SC Signal with SISO Channel.....	38
5.3.1	Transmission Result of SC QPSK Signal (SISO).....	38
5.3.2	Transmission Result of SC 8-QAM Signal (SISO).....	40
5.3.3	Transmission Result of SC 16-QAM Signal (SISO).....	41
5.4	Experimental Result for SC Signal with MIMO Technology	41
5.4.1	SC MIMO Signal at Different FFT Size of FDE.....	42
5.4.2	SC MIMO Signal at Different CP Length of FDE.....	44
5.4.3	SC MIMO Signal at Different Channel Correlation	45
5.4.4	Transmission Result of SC QPSK Signal (MIMO).....	46
5.4.5	Transmission Result of SC 8-QAM Signal (MIMO)	47
5.4.6	Transmission Result of SC 16-QAM Signal (SISO).....	49
Chapter 6	Conclusion	51
References	52

List of Figures

Figure 1-1	The allocated band and bandwidth in the U.S.A.....	2
Figure 2-1	the concept of RoF system with MIMO technology.....	5
Figure 2-2	time diversity.....	7
Figure 2-3	2x1 MISO.....	8
Figure 2-4	2x1 Alamouti space-time code.....	10
Figure 2-5	simulation result of Alamouti space-time code.....	10
Figure 2-6	MIMO channel converts into parallel channel.....	12
Figure 2-7	2x2 spatial multiplexing MIMO.....	14
Figure 2-8	the correlated channel.	15
Figure 2-9	simulation result of MIMO with ZF receiver.....	15
Figure 2-10	simulation result of MIMO with ML receiver.....	17
Figure 3-1	the basic ideal of FDE.....	22
Figure 3-2	the block diagram of FDE.....	22
Figure 3-3	2x2 MIMO RoF system.....	23
Figure 3-4	the block diagram of 2x2 MIMO with FDE..	24
Figure 4-1	Single-electrode Mach-Zehnder Modulator.....	28
Figure 4-2	the different order of Bessel function versus m.	29
Figure 4-3	the concept of the proposed system..	32
Figure 4-4	Magnitude of Bessel functions versus different modulation index..	34
Figure 5-1	experimental setup of the propose system..	37
Figure 5-2	optical spectrum for 16 QAM SC signal.....	37
Figure 5-3	electrical spectrum for 16 QAM SC signal.....	38
Figure 5-4	BER curve of QPSK SC signal with SISO channel.....	39
Figure 5-5	Constellations of the QPSK SC signal with SISO channel.....	39
Figure 5-6	BER curve of 8-QAM SC signal with SISO channel..	40

Figure 5-7	Constellations of the 8-QAM SC signal with SISO channel..	41
Figure 5-8	BER curve of 16-QAM SC signal with SISO channel..	41
Figure 5-9	Constellations of the 8-QAM SC signal with SISO channel..	42
Figure 5-10	BER curve of 16-QAM SC signal with MIMO channel in BTB transmission at different FFT size.....	43
Figure 5-11	BER curve of 16-QAM SC signal with MIMO channel in BTB transmission at different CP length.....	44
Figure 5-12	SNR versus MIMO Channel correlation of 16-QAM SC signal in BTB transmission.....	45
Figure 5-13	BER curve of QPSK SC signal with MIMO channel..	46
Figure 5-14	Constellations of the QPSK MIMO signal..	47
Figure 5-15	BER curve of 8-QAM SC signal with MIMO channel.....	48
Figure 5-16	Constellations of the 8-QAM MIMO signal.....	48
Figure 5-17	BER curve of 16-QAM SC signal with MIMO channel.....	49
Figure 5-18	Constellations of the 16-QAM MIMO signal.....	50



Chapter 1

Introduction

1.1 Background

With the rapid growth of technology, people have been from computer generation to the internet generation. Many kinds of internet products, such as smart phone, tablet PC, and various internet services, like facebook, twitter, high-definition images, are developed rapidly in the recent years. Peoples' life and internet have been combined closely. People need the internet everywhere, even on the bus, on the train, on the way to somewhere. Thus, the wireless communication becomes more and more important today.

In order to support such internet services, the speed of data transmission must improve. However, the most popular communication standards, such as 3G, 4G and WiFi don't have enough commercial wireless communication bandwidth, and the data rate can't exceed 1Gbit/s. The carrier frequency of the wireless signal has to be raised to break the limitation of bandwidth. The allocation of communication band and bandwidth are different from different countries, and Figure 1-1 shows that the band and the bandwidth are allowed to use in the USA. After U.S. Federal Communications opened bands with 50-120 GHz, there are several bands above 50GHz which have large enough bandwidths to support high-speed data transmission (57-64GHz, 71-76GHz, 81-86GHz and 92-95GHz). And the band at 60 GHz which have 7 GHz unlicensed bandwidth is attractive to the industry and the research [1-3].

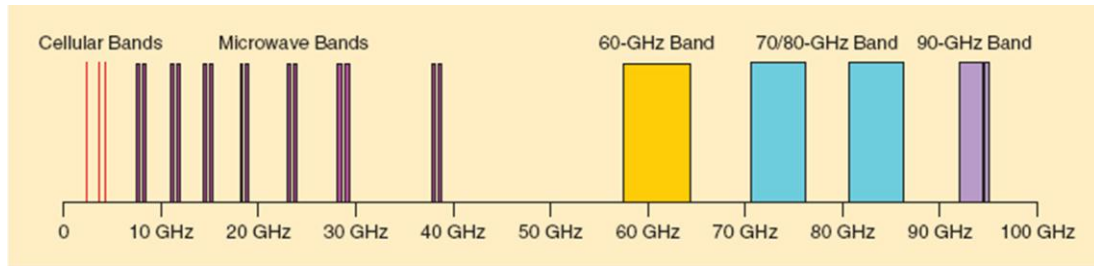


Figure 1-1 The allocated band and bandwidth in the U.S.A.

Due to the physical property of the transmission wave, the transmission distance will decrease when the carrier frequency increase. Because of the smaller coverage area, we need more base stations than using lower carrier frequency to support the same service region. The signal loss will be the main problem when high-frequency signal is transmitted by the coaxial cable, and second problem is the cost issue that the price of high-frequency coaxial cable is very high. Thus, Radio-over-Fiber (RoF) system [4] was proposed to solve the power and cost issues in the millimeter-wave signals.

Using fiber as the transmission medium is one of the best solution because there is not only unlimited bandwidth but also less power loss in fiber. RoF system can save the system cost by reducing the equipment of base stations (BSs) along with highly centralized central station (CS) equipped with optical and mm-wave components.

1.2 Motivation

Due to the demand for higher bandwidth, MIMO technology [5-7] becomes the most attractive solution to increase the bandwidth efficiency. Thus, MIMO technology has been used in many communication standards for recent years. Table 1-1 [8] shows various wireless communication standards,

and several standards such as WiMax, LTE, WiFi and so on, have involved MIMO technology. Hence, MIMO transmission technology will play an important role to the development of the wireless communication in the future.

Standard	Family	Primary Use	Radio Tech	Downlink (Mbit/s)	Uplink (Mbit/s)
WiMAX	802.16	Mobile Internet	MIMO-SOFDMA	128 (in 20MHz bandwidth)	56 (in 20MHz bandwidth)
LTE	UMTS/4GSM	General 4G	OFDMA/MIMO/S C-FDMA	100 (in 20MHz bandwidth)	50 (in 20 MHz bandwidth)
Flash-OFDM	Flash-OFDM	Mobile Internet	Flash-OFDM	5.3	1.8
		mobility up to 200mph (350km/h)		10.6	3.6
				15.9	5.4
HIPERMAN	HIPERMAN	Mobile Internet	OFDM	56.9	
Wi-Fi	802.11(11n)	Mobile Internet	OFDM/MIMO	300 (using 4x4 configuration in 20MHz bandwidth) or 600 (using 4x4 configuration in 40MHz bandwidth)	
iBurst	802.2	Mobile Internet	HC-SDMA/TDD/MIMO	95	36
EDGE Evolution	GSM	Mobile Internet	TDMA/FDD	1.6	0.5
UMTS W-CDMA HSDPA+HSUPA HSPA+	UMTS/3GSM	General 3G	CDMA/FDD	0.384	0.384
				14.4	5.76
			CDMA/FDD/MIMO	56	22
UMTS-TDD	UMTS/3GSM	Mobile Internet	CDMA/TDD	16	
1xRTT	CDMA2000	Mobile phone	CDMA	0.144	
EV-DO 1x Rev. 0 EV-DO 1x Rev.A EV-DO Rev.B	CDMA2000	Mobile Internet	CDMA/FDD	2.45 3.1 4.9xN	0.15 1.8 1.8xN

Table 1-1 wireless communication standards

1.3 Objection and Problem Statement

In this thesis, we will demonstrate the 60 GHz RoF system using 2×2 MIMO technology transmitting the Single Carrier vector signal to increase the spectrum efficiency in the 7 GHz unlicensed band. However, there are two main problems we will meet.

The first challenge is non-flat channel response with up to 10dB deviation within the 7 GHz spectrum. The 7 GHz SC signal will have a serious ISI problem. The complexity of the MIMO process in the time domain will rapidly increase. To overcome this problem, the SC frequency domain equalizer (FDE) [9] is used. FDE not only can compensate the uneven channel response but also can well separate the MIMO signals in the frequency domain.

The second one is the noise enhancement because of MIMO channel correlation. Channel correlation between different transmitted antennas is very important to the signal performance in the light of sight (LOS) MIMO scenario. The channel correlation is related to the distance and the angles of received signals. The problem can be solved by increasing the antenna pairs or introducing the concept of the smart antennas where we don't focus on this topic in this thesis. The channel correlation can also be decreased by well adjusting the antenna spacing.

Chapter 2

Multiple-Input Multiple-Output (MIMO) Technology

2.1 Preface

The RoF system is the possible solution of the high data rate wireless transmission in the future because of the property of the fiber which is low loss and have almost unlimited bandwidth. However, the bandwidth in wireless communication is constrained by the law. In order to raise the data rate in the fixed bandwidth, MIMO is the effective way to improve the spectrum efficiency. Figure 2-1 shows the RoF system with the MIMO technology. In this chapter, we will introduce the basic concept of MIMO.

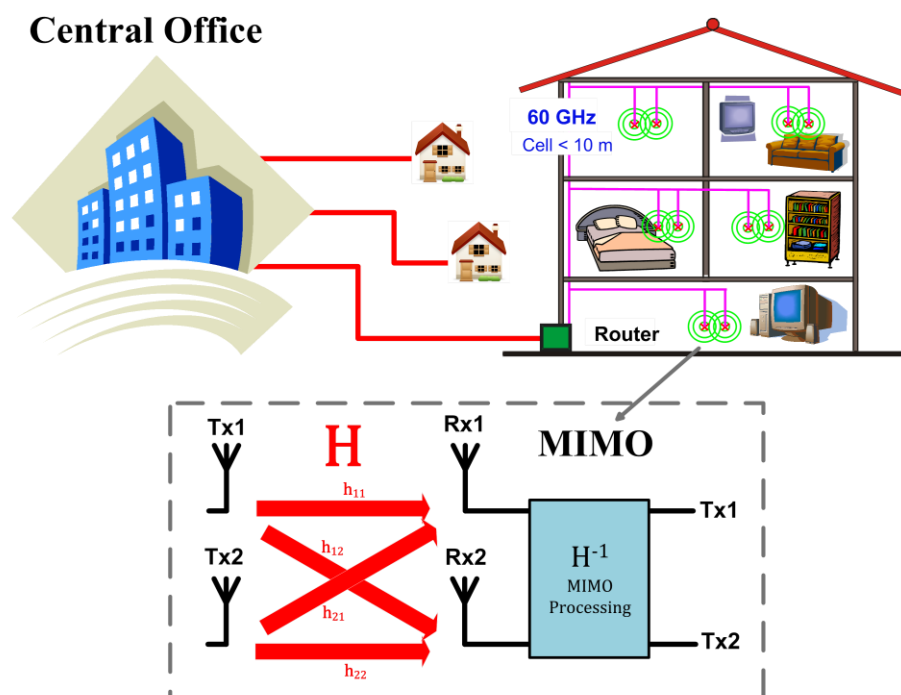


Figure 2-1 the concept of RoF system with MIMO technology.

2.2 MIMO Technology for Improving Performance

2.2.1 Diversity

In the non-LOS wireless communication, we don't know how the signal is received from transmitter to the receiver. The signal may be reflected, scattered, refracted and even blocked on the way to the receiver. If the signal performance is so poor that can't be the reliable communication, we call this path is in a deep fade. When the path is in a deep fade, the communication will suffer from errors. A technique is called diversity, and it can significantly improve the performance over the fading channels.

There are many ways to obtain diversity, we introduce three diversity techniques in time, frequency and space in the chapter. Figure 2-2 shows the concept of the time diversity. H is a fading channel variously with time. When the time block 3 is in a deep fade, the signal at time block 3 will suffer from error. Now, the same signal x is transmitted three times. Thus, even if the time block 3 is in deep fade, the signal x still could be detected correctly depending the received signals at other two time blocks. Similarly, one can also exploit diversity over frequency if the channel is frequency-selective which means the channel changes variously with the frequency. Multiple transmit and receive antennas will create the different channels from the different transmit antennas to receive antennas. The same signal can be received many times because of the different transmit paths, and the spatial diversity is obtained. The diversity technique is an important resource to the wireless communication, and we will introduce the Alamouti space-time code to implement the space diversity to improve the signal performance in next section.

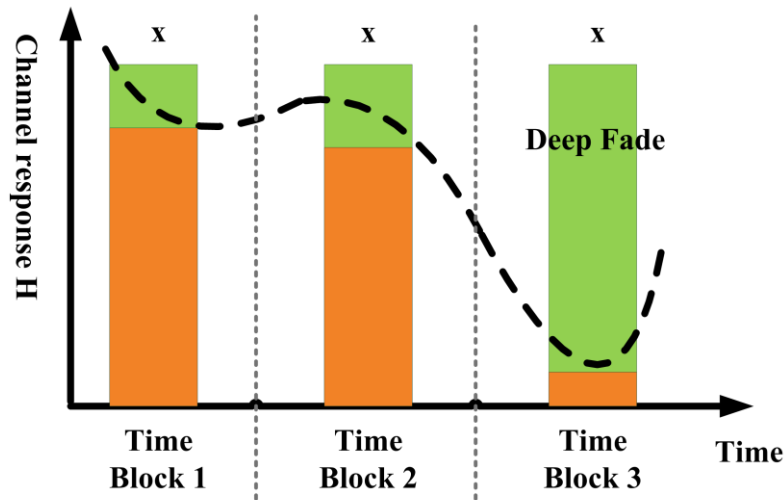


Figure 2-2 time diversity.

2.2.2 Alamouti Space-Time Code

Spatial diversity which we can also call it antenna diversity, it involves both the receive diversity, using multiple receive antennas (single input multiple output, SIMO channels), and the transmit diversity, using multiple transmit antennas (multiple input single output, MISO channels). Channels with multiple transmit antennas and multiple receive antennas (multiple input multiple output, MIMO channels) provide more potential.

Alamouti scheme was proposed by Mr. Siavash M Alamouti in his landmark paper – A Simple Transmit Diversity Technique for Wireless Communication. This is the transmit diversity scheme proposed in several third-generation cellular standards. The Alamouti scheme is designed for two transmit antennas at the first, but more than two transmit antennas is possible. For the discussion, we will assume that the channel is a flat fading Rayleigh multipath channel.

Figure 2-3 shows a 2 x 1 MISO scenario, and there are two transmit antennas and one receive antenna. Two transmitted signals x_1 and x_2 are

transmitted to the receive antenna and the received signal y is written as

$$y[m] = h_1[m]x_1[m] + h_2[m]x_2[m] + w[m] \quad (\text{Eq. 2-1})$$

Where h_i is the channel gain from transmit antenna i , and w is the additive white Gaussian noise (AWGN).

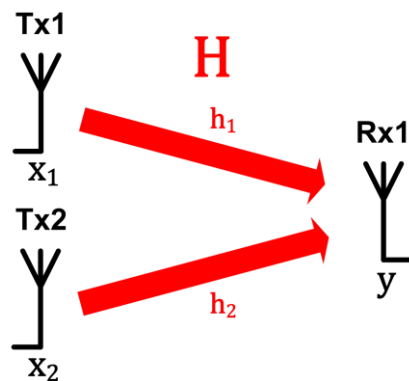


Figure 2-3 2x1 MISO

Now, we have a transmission sequence such as $\{u_1, u_2, u_3, u_4, \dots\}$ which are the data symbols. In the normal transmission, we will transmit u_1 in the first time slot, u_2 in the second time slot, u_3 in the third time slot and so on. However, The Alamouti scheme transmits two symbols u_1 and u_2 over two times. At time slot 1, $x_1[1] = u_1, x_2[1] = u_2$; At time slot 2, $x_1[2] = -u_2^*, x_2[2] = u_1^*$; We assume that the channel remain constant over the two symbol times which $h_1 = h_1[1] = h_1[2], h_2 = h_2[1] = h_2[2]$, as the figure 2-4 shown, 2 x 1 Alamouti space-time code. Then, the receive signal can be expressed as

$$\begin{bmatrix} y[1] \\ y[2] \end{bmatrix} = \begin{bmatrix} h_1 & h_2 \end{bmatrix} \begin{bmatrix} u_1 & -u_2^* \\ u_2 & u_1^* \end{bmatrix} + \begin{bmatrix} w[1] \\ w[2] \end{bmatrix} \quad (\text{Eq. 2-2})$$

The equation can be rewrote as

$$\begin{bmatrix} y[1] \\ y[2]^* \end{bmatrix} = \begin{bmatrix} h_1 & h_2 \\ h_2^* & -h_1^* \end{bmatrix} \begin{bmatrix} u_1 \\ u_2 \end{bmatrix} + \begin{bmatrix} w[1] \\ w[2]^* \end{bmatrix} \quad (\text{Eq. 2-3})$$

Let us define

$$\mathbf{H} = \begin{bmatrix} h_1 & h_2 \\ h_2^* & -h_1^* \end{bmatrix} \quad (\text{Eq. 2-4})$$

The channel coefficients h_1, h_2 have known. To solve for u_1, u_2 , we multiple the Hermitian matrix of \mathbf{H} to the $[y[1] \ y[2]^*]^T$

$$\mathbf{H}^H = \begin{bmatrix} h_1^* & h_2 \\ h_2^* & -h_1^* \end{bmatrix} \quad (\text{Eq. 2-5})$$

$$\begin{bmatrix} r_1 \\ r_2 \end{bmatrix} = \mathbf{H}^H \begin{bmatrix} y[1] \\ y[2]^* \end{bmatrix} = \begin{bmatrix} h_1^* & h_2 \\ h_2^* & -h_1^* \end{bmatrix} \begin{bmatrix} h_1 & h_2 \\ h_2^* & -h_1^* \end{bmatrix} \begin{bmatrix} u_1 \\ u_2 \end{bmatrix} + \mathbf{H}^H \begin{bmatrix} w[1] \\ w[2]^* \end{bmatrix} \quad (\text{Eq. 2-6})$$

$$\begin{bmatrix} r_1 \\ r_2 \end{bmatrix} = \begin{bmatrix} |h_1|^2 + |h_2|^2 & 0 \\ 0 & |h_1|^2 + |h_2|^2 \end{bmatrix} \begin{bmatrix} u_1 \\ u_2 \end{bmatrix} + \mathbf{H}^H \begin{bmatrix} w[1] \\ w[2]^* \end{bmatrix} \quad (\text{Eq. 2-7})$$

The estimate of transmit symbols are by inverting the diagonal matrix

$$(\mathbf{H}^H \mathbf{H})^{-1} = \begin{bmatrix} \frac{1}{|h_1|^2 + |h_2|^2} & 0 \\ 0 & \frac{1}{|h_1|^2 + |h_2|^2} \end{bmatrix} \quad (\text{Eq. 2-8})$$

$$\begin{bmatrix} \hat{u}_1 \\ \hat{u}_2 \end{bmatrix} = (\mathbf{H}^H \mathbf{H})^{-1} \begin{bmatrix} r_1 \\ r_2 \end{bmatrix} + (\mathbf{H}^H \mathbf{H})^{-1} \mathbf{H}^H \begin{bmatrix} w[1] \\ w[2]^* \end{bmatrix} \quad (\text{Eq. 2-9})$$

$$\begin{bmatrix} \hat{u}_1 \\ \hat{u}_2 \end{bmatrix} = \begin{bmatrix} u_1 \\ u_2 \end{bmatrix} + (\mathbf{H}^H \mathbf{H})^{-1} \mathbf{H}^H \begin{bmatrix} w[1] \\ w[2]^* \end{bmatrix} \quad (\text{Eq. 2-10})$$

Thus, the transmit diversity gain is 2 for the detection of each symbol. It is possible to provide diversity order $2M$ with two transmit and M receive antennas. Figure 2-5 is the simulation result of 2×2 Alamouti scheme where

the channel is the flat fading Rayleigh channel, and the noise is AWGN. Clearly, 2 x 2 Alamouti scheme has better performance than the SISO channel.

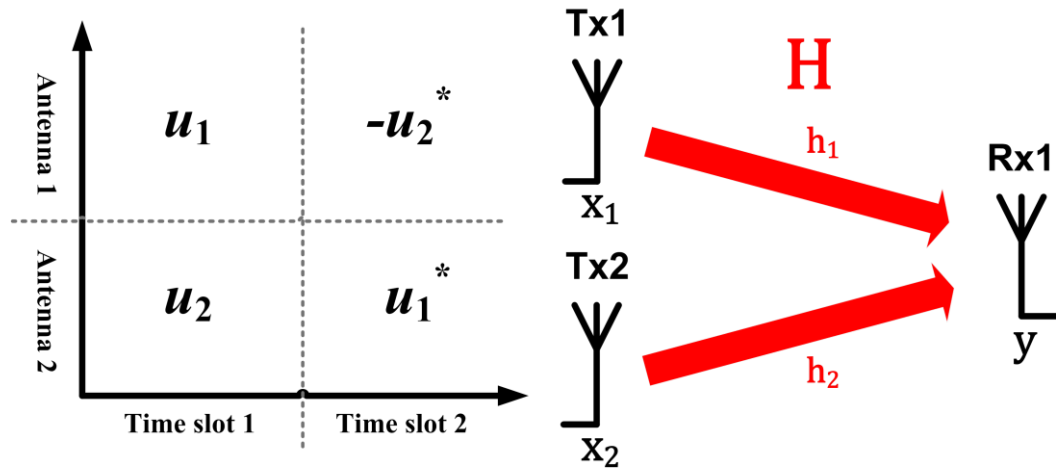


Figure 2-4 2x1 Alamouti space-time code.

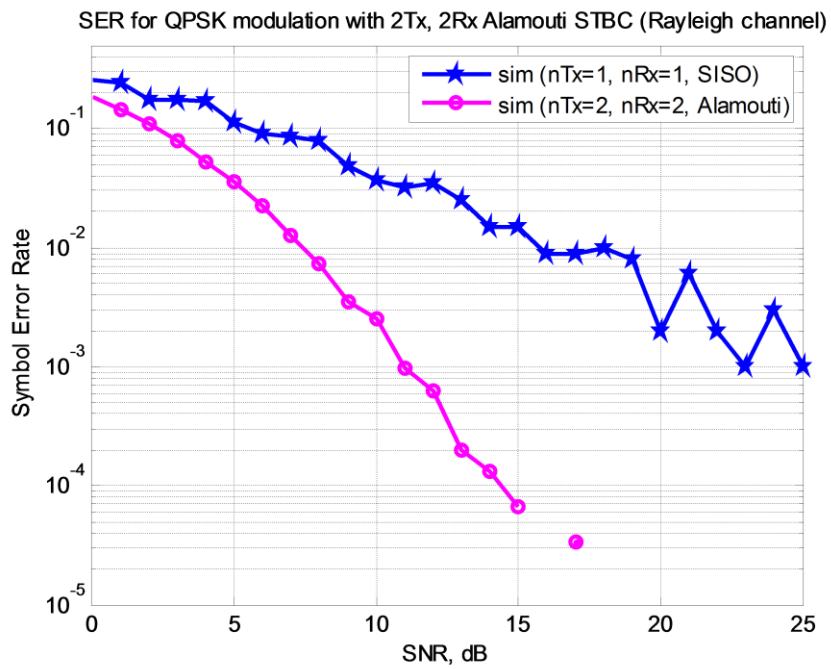


Figure 2-5 simulation result of Alamouti space-time code.

2.3 MIMO Technology for Improving Capacity

We will see that under suitable channel conditions, MIMO channel provides an additional spatial dimension for communication and degrees of

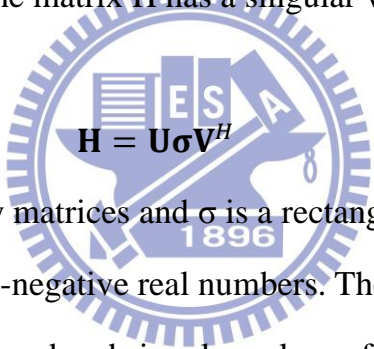
freedom. These additional degrees of freedom can be exploited by spatial multiplexing several data streams on to the MIMO channel and the overall capacity is increased.

The time-invariant MIMO channel with n_t transmit and n_r receive antennas can be written as the n_r by n_t deterministic matrix \mathbf{H}

$$\mathbf{y} = \mathbf{H}\mathbf{x} + \mathbf{w} \quad (\text{Eq. 2-11})$$

where \mathbf{x} , \mathbf{y} and \mathbf{w} denote the transmitted signal, received signal and white Gaussian noise at a symbol time.

This is a vector Gaussian channel. The capacity can be computed by decomposing the vector channel into a set of parallel, independent scalar Gaussian sub-channels. The matrix \mathbf{H} has a singular value decomposition (SVD):



$$\mathbf{H} = \mathbf{U}\boldsymbol{\sigma}\mathbf{V}^H \quad (\text{Eq. 2-12})$$

where \mathbf{U} and \mathbf{V} are unitary matrices and $\boldsymbol{\sigma}$ is a rectangular matrix whose diagonal elements are non-negative real numbers. The diagonal elements $\lambda_1 \geq \lambda_2 \geq \dots \geq \lambda_{n_{\min}}$ are the ordered singular values of matrix \mathbf{H} , where $n_{\min} = \min(n_t, n_r)$. We can rewrite the SVD as

$$\mathbf{H} = \sum_{i=1}^{n_{\min}} \lambda_i \mathbf{u}_i \mathbf{v}_i^H \quad (\text{Eq. 2-13})$$

The sum of rank-one matrices $\lambda_i \mathbf{u}_i \mathbf{v}_i^H$. It can be seen that the rank of \mathbf{H} is the number of non-zero singular values.

If we define

$$\tilde{\mathbf{x}} = \mathbf{V}^H \mathbf{x} \quad (\text{Eq. 2-14})$$

$$\tilde{\mathbf{y}} = \mathbf{U}^H \mathbf{y} \quad (\text{Eq. 2-15})$$

$$\tilde{\mathbf{w}} = \mathbf{U}^H \mathbf{w} \quad (\text{Eq. 2-16})$$

then we can rewrite the channel as

$$\tilde{\mathbf{y}} = \boldsymbol{\sigma} \tilde{\mathbf{x}} + \tilde{\mathbf{w}} \quad (\text{Eq. 2-17})$$

Then, we have an equivalent representation as parallel Gaussian channel

$$\tilde{y}_i = \lambda_i \tilde{x}_i + \tilde{w}_i, \quad i = 1, 2, \dots, n_{\min} \quad (\text{Eq. 2-18})$$

Figure 2-6 shows the equivalence.

We can look the SVD decomposition as two coordinate transformations. If the input is expressed in terms of coordinate system defined by the columns of \mathbf{V} and the output is expressed in terms of a coordinate system defined by the column \mathbf{U} , then the relationship between input and output can be very simple. Thus, the property of MIMO channel will dominate how much data we can transmit.

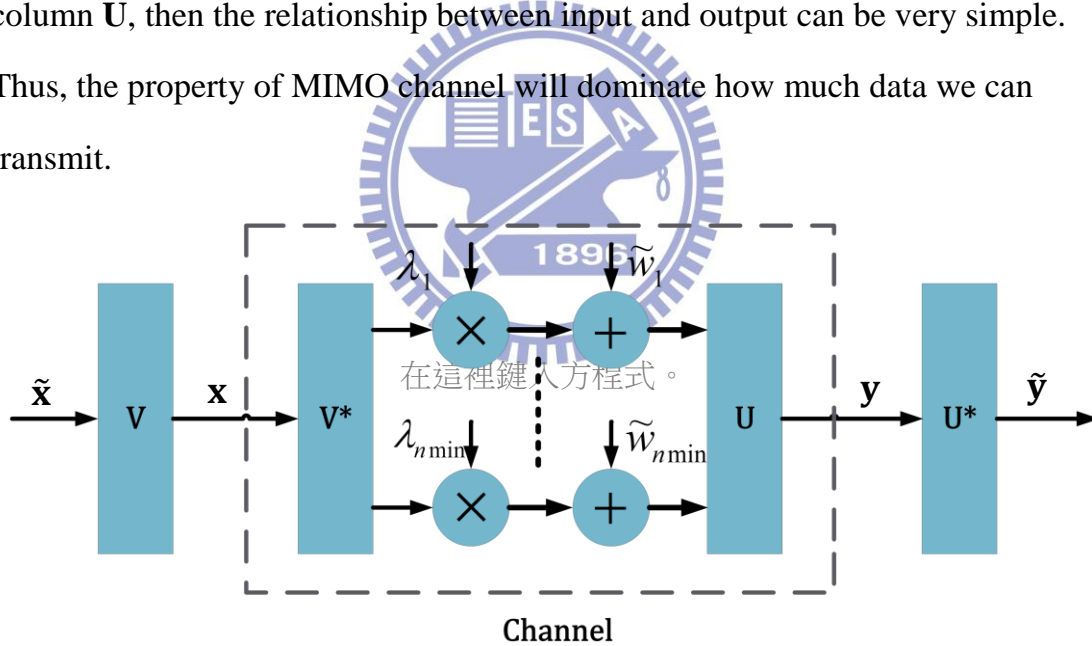


Figure 2-6 MIMO channel converts into parallel channel.

2.3.1 Spatial Multiplexing : Zero-Forcing Receiver

For a deterministic time-invariant MIMO channel, the capacity-achieving architecture is simple. Independent data streams are multiplexed in an appropriate coordinate system. The receiver transforms the received vector into

another appropriate coordinate system to separate the different data streams.

Figure 2-7 shows a 2 x2 spatial multiplexing MIMO scheme. Let's rewrite it to the matrix form as:

$$\mathbf{y} = \mathbf{H}\mathbf{x} + \mathbf{w} \quad (\text{Eq. 2-19})$$

$$\begin{bmatrix} y_1 \\ y_2 \end{bmatrix} = \begin{bmatrix} h_{11} & h_{21} \\ h_{12} & h_{22} \end{bmatrix} \begin{bmatrix} x_1 \\ x_2 \end{bmatrix} + \begin{bmatrix} w_1 \\ w_2 \end{bmatrix} \quad (\text{Eq. 2-20})$$

where \mathbf{H} is the channel matrix, and $\mathbf{x} = [x_1 \ x_2]^T$ is the input vector is consist of two independent symbols x_1, x_2 , $\mathbf{w} = [w_1 \ w_2]^T$ is the noise. Assume the element of the channel matrix is known, the transmitted data can be recovered by using the zero-forcing algorithm and written as

$$\tilde{\mathbf{y}} = \mathbf{H}^{-1}\mathbf{y} = \mathbf{x} + \mathbf{H}^{-1}\mathbf{w} = \mathbf{x} + \tilde{\mathbf{w}} \quad (\text{Eq. 2-21})$$

However, the noise \tilde{w}_1 and \tilde{w}_2 are correlated. The performance will decrease.

First, we focus on the detection of symbol form transmit antenna 1. The noise become:

$$\tilde{w}_1 = \frac{h_{22}w_1 - h_{21}w_2}{h_{11}h_{22} - h_{12}h_{21}} \quad (\text{Eq. 2-22})$$

Because of the white noise w_1 and w_2 have the same power, the noise \tilde{w}_1 can be expressed as

$$\tilde{w}_1 = \frac{\sqrt{|h_{21}|^2 + |h_{22}|^2}}{h_{11}h_{22} - h_{12}h_{21}} z_1 \quad (\text{Eq. 2-23})$$

where z_1 is white noise and the power is as same as w_1 and w_2 . Thus, we rewrite the first detect signal \tilde{y}_1 as

$$\tilde{y}_1 = x_1 + \frac{\sqrt{|h_{21}|^2 + |h_{22}|^2}}{h_{11}h_{22} - h_{12}h_{21}} z_1$$

(Eq. 2-24)

Then we define

$$y'_1 = \frac{h_{11}h_{22} - h_{12}h_{21}}{\sqrt{|h_{21}|^2 + |h_{22}|^2}} \tilde{y}_1 = (\phi_2^H \mathbf{h}_1) x_1 + z_1$$

(Eq. 2-25)

where

$$\mathbf{h}_1 = \begin{bmatrix} h_{11} \\ h_{12} \end{bmatrix}, \quad \phi_2 = \frac{1}{\sqrt{|h_{21}|^2 + |h_{22}|^2}} \begin{bmatrix} h_{22}^* \\ -h_{21}^* \end{bmatrix}$$

(Eq. 2-26)

The \mathbf{h}_1 can be seen as the direction of the signal from transmit antenna 1, and the ϕ_2 is the direction orthogonal to \mathbf{h}_2 . Equation 2-25 represents that the signal from transmit antenna 1 is detected by projecting the received signal y to the direction perpendicular to the direction of the transmit antenna 2, \mathbf{h}_2 . Hence, the interference from transmit antenna 2 can be eliminated. However, if the \mathbf{h}_1 and \mathbf{h}_2 are not orthogonal in the beginning, the vector of \mathbf{h}_1 orthogonal to the \mathbf{h}_2 will be smaller than \mathbf{h}_1 itself as figure 2-8 shown.

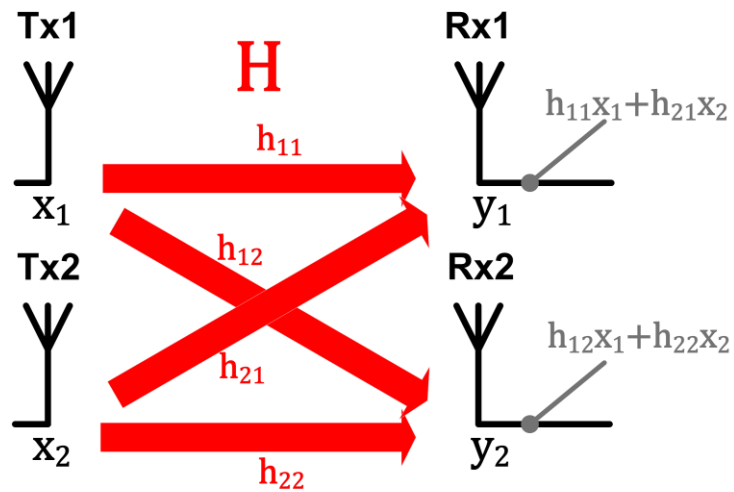


Figure 2-7 2x2 spatial multiplexing MIMO.

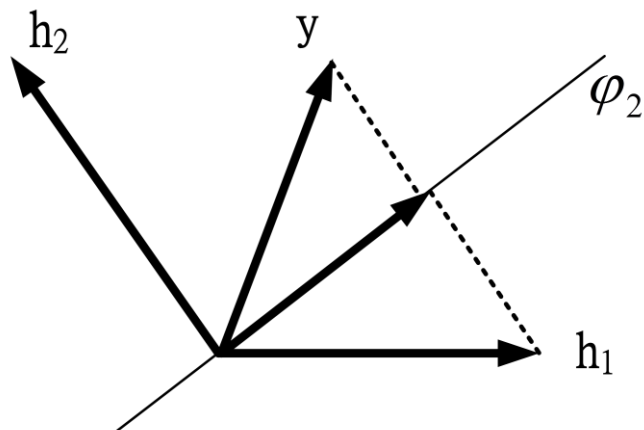


Figure 2-8 the correlated channel.

Figure 2-9 is the simulation result of 2x2 MIMO channel with Zero-Forcing receiver where the channel is the flat fading Rayleigh channel, and the noise is AWGN and the transmit antennas transmit two independent symbols at once. We only use the one dimension to decode the signal by the projection, so we don't have any diversity gain in this scheme. Thus, the performance is not better to the SISO channel, but the capacity is double.

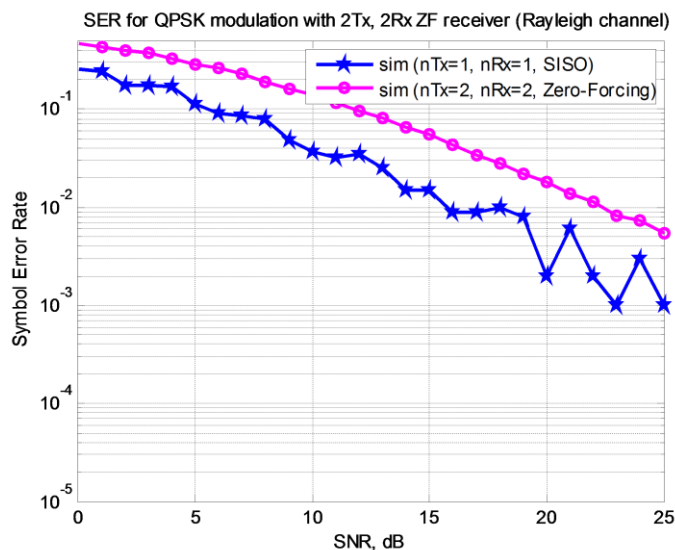


Figure 2-9 simulation result of MIMO with ZF receiver.

2.3.2 Spatial Multiplexing : Maximum-Likelihood Receiver

Maximum-Likelihood (ML) receiver is the very directly way to detect the independent data streams. The core idea of the ML detection is to compare all of the possible transmitted symbols to find the maximum likely one. Figure 2-7 is the 2x2 spatial multiplexing MIMO scheme. Equation 2-19 and Equation 2-20 is the matrix form of this scheme, where \mathbf{H} is the channel matrix, and $\mathbf{x} = [x_1 \ x_2]^T$ is the input vector is consist of two independent symbols x_1, x_2 , $\mathbf{w} = [w_1 \ w_2]^T$ is white noise. The ML detection bases on the following equation:

$$\mathbf{s} = \arg \min_{\mathbf{x}} \|\mathbf{y} - \mathbf{H}\hat{\mathbf{x}}\|^2 \quad (\text{Eq. 2-27})$$

Assume the channel matrix \mathbf{H} is known, and we also know what kind of the symbol $\hat{\mathbf{x}}$ the transmit antenna may sent. Then, the receiver can decision what kind of symbol it is.

For an example, the 2x2 MIMO scheme is like figure 2-7, and the modulation is BPSK. The ML receiver tries to find $\hat{\mathbf{x}}$ which minimizes $\mathbf{K} = \|\mathbf{y} - \mathbf{H}\hat{\mathbf{x}}\|^2$, and the possible value of the BPSK symbol is +1 or -1. So we need to find the minimum from all four possible combinations.

$$\mathbf{K}_{+1,+1} = \left\| \begin{bmatrix} y_1 \\ y_2 \end{bmatrix} - \begin{bmatrix} h_{11} & h_{21} \\ h_{12} & h_{22} \end{bmatrix} \begin{bmatrix} +1 \\ +1 \end{bmatrix} \right\|^2 \quad (\text{Eq. 2-28})$$

$$\mathbf{K}_{+1,-1} = \left\| \begin{bmatrix} y_1 \\ y_2 \end{bmatrix} - \begin{bmatrix} h_{11} & h_{21} \\ h_{12} & h_{22} \end{bmatrix} \begin{bmatrix} +1 \\ -1 \end{bmatrix} \right\|^2 \quad (\text{Eq. 2-29})$$

$$\mathbf{K}_{-1,+1} = \left\| \begin{bmatrix} y_1 \\ y_2 \end{bmatrix} - \begin{bmatrix} h_{11} & h_{21} \\ h_{12} & h_{22} \end{bmatrix} \begin{bmatrix} -1 \\ +1 \end{bmatrix} \right\|^2 \quad (\text{Eq. 2-30})$$

$$\mathbf{K}_{-1,-1} = \left\| \begin{bmatrix} y_1 \\ y_2 \end{bmatrix} - \begin{bmatrix} h_{11} & h_{21} \\ h_{12} & h_{22} \end{bmatrix} \begin{bmatrix} -1 \\ -1 \end{bmatrix} \right\|^2 \quad (\text{Eq. 2-31})$$

If the minimum is $\mathbf{K}_{+1,+1}$, the estimate transmitted symbol $\hat{\mathbf{x}}$ is [+1,+1]. Due to all of the dimensions are considered, the performance is better than the SISO channel by the diversity gain. Figure 2-10 shows the simulation result.

However, the complexity of the ML receiver will exponentially grow with

increasing the number of antennas and the order of data format of symbols.

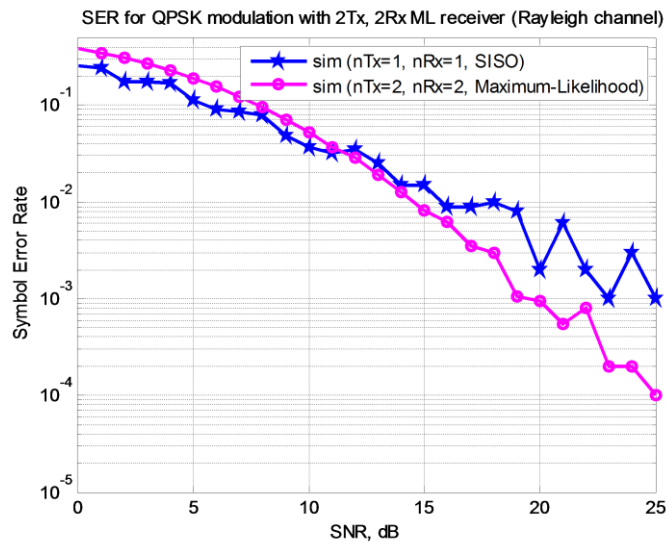
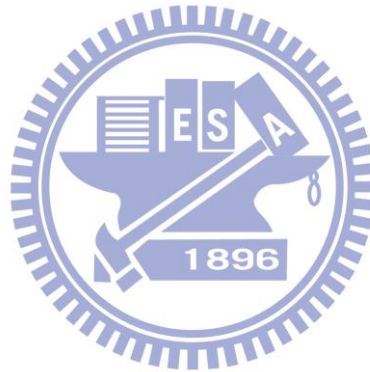


Figure 2-10 simulation result of MIMO with ML receiver.



Chapter 3

Single Carrier Frequency Domain Equalizer

3.1 Preface

In this thesis, we want to apply the MIMO antenna technology to the 60 GHz RoF system with 7 GHz broadband bandwidth doubling the data rate. However, such high carrier frequency signal (60 GHz) has very high propagation losses rendering it more suitable for short-range wireless links (~10m). The wideband 60 GHz RoF system has an uneven frequency response of up to 12 dB within 7 GHz license-free band. These two properties make the MIMO channel in 60 GHz RoF system is a time-invariant and frequency-selective channel. Hence, it is the different situation from the assumption in the chapter 2. We assume the MIMO channel is a flat fading Rayleigh channel in the chapter 2. In this chapter, the complexity will highly increase by using the ZF detector due to the frequency-selective channel, but we will introduce the frequency domain equalizer (FDE) to MIMO technology which is simple method to double the data rate.

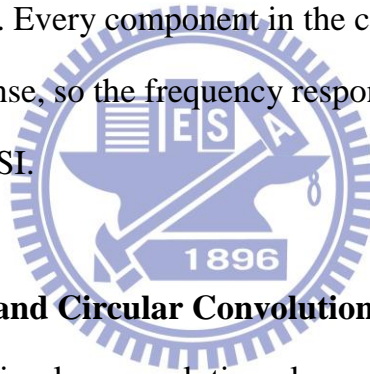
3.2 Inter-Symbol Interference

Inter-symbol interference is an important issue in digital communication. It is a form of distortion of signal where the symbols interfere to the symbols each other. That's just like the noise to the decision samples, and that will make the communication less reliable. ISI usually comes from two different situations. One is the multipath propagation, and the other one is the uneven

frequency response of the system.

ISI of the multipath propagation occurs because of the wireless signal from the transmit antenna to the receive antenna via different paths. The same signal will arrive to the receiver at different time due to the various paths, so the signals are going to distort the amplitude and phase which cause interference between symbols at different time. The phenomenon of fiber dispersion also results in ISI. The reason is similar to the multipath propagation.

Compared to the ISI of the multipath propagation, the ISI because of the uneven frequency response of the system is presented in both wired and wireless communication. Every component in the communication system has its own frequency response, so the frequency response of the entire system is non-flat and will cause ISI.



3.3 Linear Convolution and Circular Convolution

The concept of the circular convolution plays an important role to the SC FDE. In this section, we will introduce from the linear convolution to the circular convolution [11].

The linear convolution of two sequences $x_1[n]$ of N_1 -point and $x_2[n]$ of N_2 -point is given by

$$x_3[n] = x_1[n] * x_2[n] = \sum_{k=-\infty}^{\infty} x_1[k] x_2[n - k] = \sum_{k=0}^{N_1-1} x_1[k] x_2[n - k] \quad (\text{Eq. 3-1})$$

where $x_3[n]$ is a $(N_1 + N_2 - 1)$ -point sequence. Now, the same sequences $x_1[n]$ and $x_2[n]$, and we choose $N = \max(N_1, N_2)$ to compute the N -point circular

convolution

$$x_4[n] = x_1[n] \otimes x_2[n] = \sum_{m=0}^{N-1} x_1[m] x_2([n - m])_N$$

(Eq. 3-2)

where $x_4[n]$ is a N -point sequence. Assume we choose $N = (N_1 + N_2 - 1)$ -point to do the circular convolution, $x_4[n]$ becomes

$$\begin{aligned} x_4[n] &= x_1[n] \otimes x_2[n] = \sum_{m=0}^{N-1} x_1[m] x_2([n - m])_N \\ &= \sum_{m=0}^{N-1} x_1[m] \sum_{r=-\infty}^{\infty} x_2[n - m - rN] \\ &= \sum_{r=-\infty}^{\infty} \sum_{m=0}^{N-1} x_1[m] x_2[n - m - rN] \\ &= \sum_{r=-\infty}^{\infty} x_3[n - rN] \end{aligned}$$

(Eq. 3-3)

Then

$$x_4[n] = x_3[n] \quad 0 \leq n \leq N - 1 \quad \text{(Eq. 3-4)}$$

Thus, the circular convolution is the aliased version of the linear convolution.

On the other hand, if we pad the number of zeros to make $x_1[n]$ and $x_2[n]$ become a $(N_1 + N_2 - 1)$ -point sequence, the result of circular convolution is equal to the result of linear convolution.

3.4 Single Carrier Frequency Domain Equalizer

The traditional method to compensate for ISI is to use a time domain equalizer at the receiver. One or more transversal filters are main components

where the number of adaptive tap coefficients is on the order of number of the data symbols spanned by ISI. An SC system transmits a single carrier modulated with QAM at high symbol rate suffering a serious ISI problem. The complexity and digital processing speed become exorbitant, and the time domain equalizer becomes unattractive.

Frequency domain equalizer compensates the channel response in the frequency domain. Figure 3-1 shows the basic idea of FDE. When a signal x into the system which the channel impulse response is h , we know that it is the convolution of the signal x and the channel h in the time domain. The convolution process becomes the simple multiplication in the frequency domain where $F\{\}$ and $F^{-1}\{\}$ are the fast Fourier transform and inverse Fourier transform, and we can easily use one tap equalizer to compensate the signal in the frequency domain. For channel with severe ISI, frequency domain equalization is computationally simpler than the time domain equalizer. Figure 3-2 is the block diagram of FDE. At first, the received signal passes the fast Fourier transform (FFT) operation transforming the time domain SC signal to frequency domain, and then the compensated signal transfer to the time domain signal by inverse fast Fourier transform (IFFT) after equalization. However, we can't do FFT to all of the data and process all of the data at once, because the memory of the digital circuit has its limitation. Thus, we want to process the signal in the block form which every M symbols ($M = 64, 128, 256 \dots$ and so on) a block. Then, the concept of cyclic prefix (CP) is introduced. CP length is L symbols which is added from the end of the data block and the length of data block becomes $M + L$ symbols at transmitter. CP makes every data block circular, and we can lead into the conception of circular convolution to equalize

M symbols at receiver after removing CP.

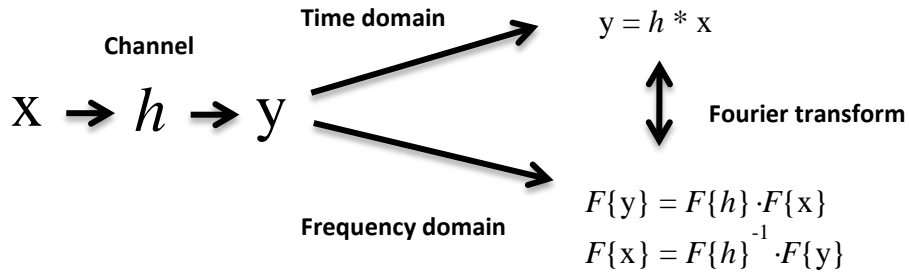


Figure 3-1 the basic ideal of FDE.

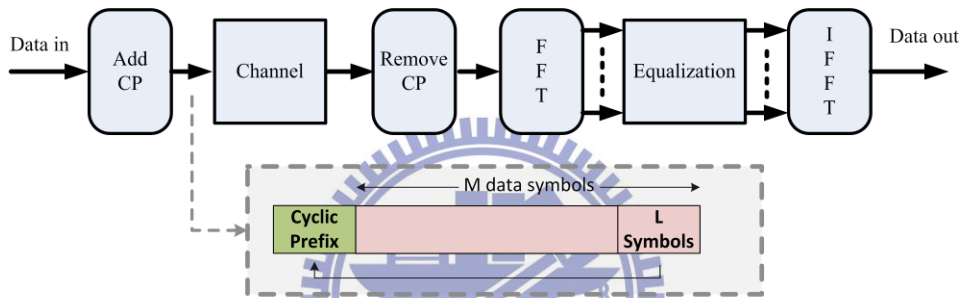


Figure 3-2 the block diagram of FDE.

3.5 MIMO Technology with Frequency Domain Equalizer

Figure 3-3 shows the fundamental concept of 2 x 2 MIMO RoF System. Two antennas, Tx1 and Tx2, transmit two different signals to the receive antennas, Rx1 and Rx2. The receive signals will be the summation of these two transmitted signals with different channel coefficients due to the different transmitting paths and can be expressed as

$$\begin{bmatrix} y_1 \\ y_2 \end{bmatrix} = \begin{bmatrix} h_{11} & h_{21} \\ h_{12} & h_{22} \end{bmatrix} \begin{bmatrix} x_1 \\ x_2 \end{bmatrix} + \begin{bmatrix} w_1 \\ w_2 \end{bmatrix} \quad (\text{Eq. 3-5})$$

where y and x are received and transmitted data, respectively, w is the noise, and h is the channel coefficient. If the channel coefficient is estimated by appropriate training symbol, the transmitted data can be recovered by using the

zero-forcing algorithm and written as

$$\begin{bmatrix} \hat{x}_1 \\ \hat{x}_2 \end{bmatrix} = \begin{bmatrix} h_{11} & h_{21} \\ h_{12} & h_{22} \end{bmatrix}^{-1} \begin{bmatrix} y_1 \\ y_2 \end{bmatrix} \quad (\text{Eq. 3-6})$$

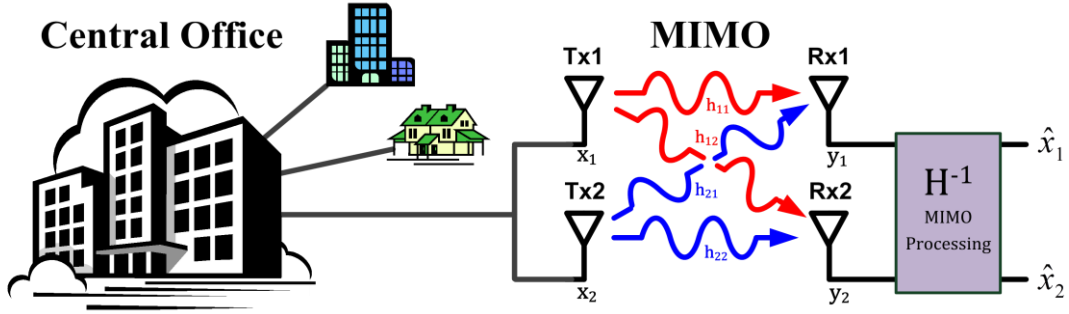


Figure 3-3 2x2 MIMO RoF system.

However, since 60 GHz RoF system has uneven frequency response of up to 12 dB within 7 GHz license-free band, the system would encounter the serious inter-symbol interference (ISI) problem. The complexity of MIMO processing in the time domain would significantly increase with the number of signal taps causing by ISI. Thus, we want to find a suitable way avoiding the highly complex matrix calculation. The proper answer is the FDE, and the received signal y transformed to the frequency domain by FFT can be expressed as

$$\begin{bmatrix} F\{y_1[m]\} \\ F\{y_2[m]\} \end{bmatrix} = \begin{bmatrix} F\{h_{11}[m]\} & F\{h_{21}[m]\} \\ F\{h_{12}[m]\} & F\{h_{22}[m]\} \end{bmatrix} \begin{bmatrix} F\{x_1[m]\} \\ F\{x_2[m]\} \end{bmatrix} + \begin{bmatrix} F\{w_1[m]\} \\ F\{w_2[m]\} \end{bmatrix} \quad m = 0, 1, \dots, M - 1 \quad (\text{Eq. 3-7})$$

Every M received symbols transform to the frequency domain by FFT. As same as the previous mentioned, the transmitted data can be recovered by using the zero-forcing algorithm, if the channel coefficients in frequency domain are estimated.

$$\begin{bmatrix} F\{\hat{x}_1[m]\} \\ F\{\hat{x}_2[m]\} \end{bmatrix} = \begin{bmatrix} F\{h_{11}[m]\} & F\{h_{21}[m]\} \\ F\{h_{12}[m]\} & F\{h_{22}[m]\} \end{bmatrix}^{-1} \begin{bmatrix} F\{y_1[m]\} \\ F\{y_2[m]\} \end{bmatrix} \quad m = 0, 1, \dots, M - 1 \quad (\text{Eq. 3-8})$$

By using the inverse fast Fourier transform $F^{-1}\{\}$, we can get the transmitted signals in the time domain and can be expressed as

$$\hat{x}_i[m] = F^{-1}\{F\{\hat{x}_i[m]\}\} \quad i = 1,2 \quad (\text{Eq. 3-9})$$

Figure 3-4 shows the block diagram for 2 x 2 MIMO systems with FDE. The bit data stream after the encoder is mapped to different data symbols. The on-off training sequence is used to estimate the channel coefficients. Each block for FDE consists of M+L symbols. Every block includes M data symbols and L symbols as cyclic prefix (CP). The data streams are transmitted to the receiver through the two transmit antennas. After other two antennas receive the transmitted data, MIMO processing is employed to compensate for uneven frequency response and recovery the data. MIMO processing includes FFT, FDE, zero-forcing algorithm, IFFT, and symbol decoder.

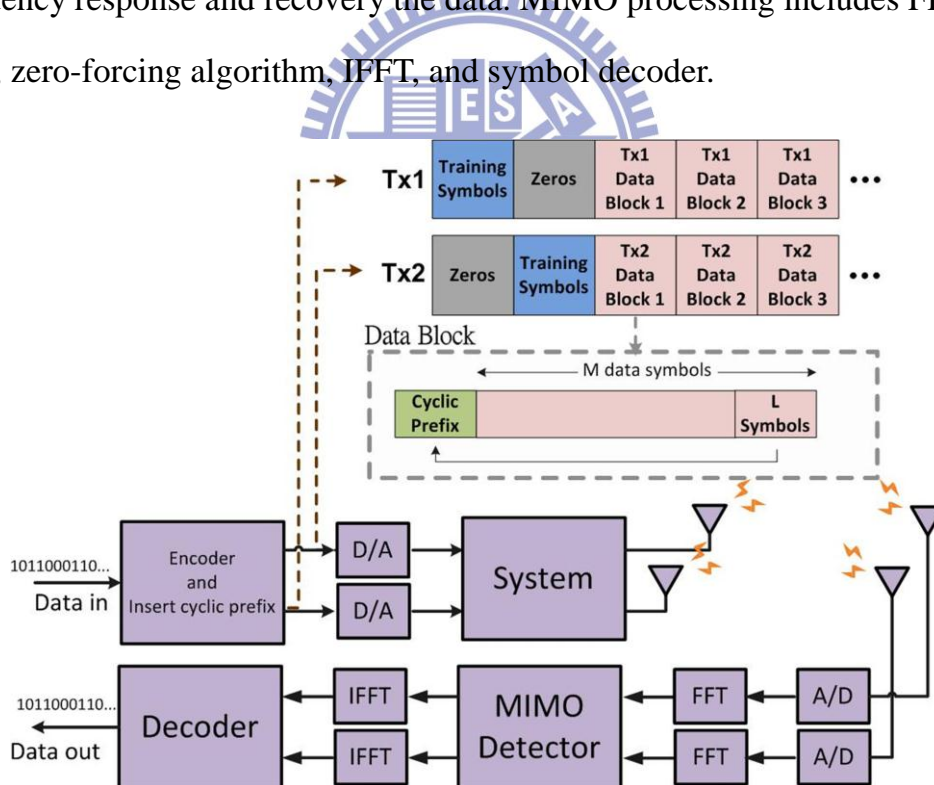


Figure 3-4 the block diagram of 2x2 MIMO with FDE.

Chapter 4

The Theoretical Calculation of Proposed System

4.1 Introduction Mach-Zehnder Modulator

Figure 4-1 shows a Mach-Zehnder Modulator (MZM), the output E-field of upper arm is

$$E_U = E_0 \cdot a \cdot e^{j\Delta\phi_1} \quad (\text{Eq. 4-1})$$

$$\Delta\phi_1 \triangleq \frac{V_1}{V_\pi} \cdot \pi \quad (\text{Eq. 4-2})$$

$\Delta\phi_1$ is the optical carrier phase difference that is induced by V_1 , where a is the power splitting ratio.

The output E-field for lower arm is

$$E_L = E_0 \cdot \sqrt{1-a^2} \cdot e^{j\Delta\phi_2} \quad (\text{Eq. 4-3})$$

$\Delta\phi_2$ is the optical carrier phase difference that is induced by V_2 ,

$$\Delta\phi_2 \triangleq \frac{V_2}{V_\pi} \cdot \pi \quad (\text{Eq. 4-4})$$

The output E-field for MZM is

$$E_T = E_0 \cdot \{a \cdot b \cdot e^{j\Delta\phi_1} + \sqrt{1-a^2} \cdot \sqrt{1-b^2} \cdot e^{j\Delta\phi_2}\} \quad (\text{Eq. 4-5})$$

where a and b are the power splitting ratios of the first and second Y-splitters in MZM, respectively. The power splitting ratio of two arms of a balanced MZM is 0.5. The electrical field at the output of the MZM is given by

$$E_T = \frac{1}{2} \cdot E_0 \cdot \{e^{j\Delta\phi_1} + e^{j\Delta\phi_2}\} \quad (\text{Eq. 4-6})$$

$$E_T = \frac{1}{2} \cdot E_0 \cdot \cos\left(\frac{\Delta\varphi_1 - \Delta\varphi_2}{2}\right) \cdot \exp\left(j \cdot \frac{\Delta\varphi_1 + \Delta\varphi_2}{2}\right) \quad (\text{Eq. 4-7})$$

For single electro x-cut MZM, the electrical field at the output is given by

$$E_{\text{out}} = E_0 \cdot \cos\left(\frac{\Delta\varphi - (-\Delta\varphi)}{2}\right) \cdot \exp\left(j \cdot \frac{\Delta\varphi + (-\Delta\varphi)}{2}\right) \quad (\text{Eq. 4-8})$$

Add time component, the electrical field is

$$E_{\text{out}} = E_0 \cdot \cos(\Delta\varphi) \cdot \exp(\omega_0 t) \quad (\text{Eq. 4-9})$$

where E_0 and ω_0 denote the amplitude and angular frequency of the input optical carrier, respectively; $V(t)$ is the applied driving voltage, and $\Delta\varphi$ is the optical carrier phase difference that is induced by $V(t)$ between the two arms of the MZM. The loss of MZM is neglected. $V(t)$ consisting of an electrical sinusoidal signal and a dc biased voltage can be written as

$$V(t) = V_{\text{bias}} + V_m \cos(\omega_{RF} t) \quad (\text{Eq. 4-10})$$

where V_{bias} is the dc biased voltage, V_m and ω_{RF} are the amplitude and the angular frequency of the electrical driving signal, respectively. The optical carrier phase difference induced by $V(t)$ is given by

$$\Delta\varphi = \frac{V(t)}{2V_\pi} = \frac{V_{\text{bias}} + V_m \cdot \cos(\omega_{RF} t)}{V_\pi} \cdot \frac{\pi}{2} \quad (\text{Eq. 4-11})$$

Equation 4-10 can be written as

$$\begin{aligned} E_{\text{out}} &= E_0 \cdot \cos\left(\frac{V_{\text{bias}} + V_m \cdot \cos(\omega_{RF} t)}{V_\pi} \cdot \frac{\pi}{2}\right) \cdot \exp(\omega_0 t) \\ &= E_0 \cdot \cos(b + m \cdot \cos(\omega_{RF} t)) \cdot \exp(\omega_0 t) \\ &= E_0 \cdot \cos(\omega_0 t) [\cos(b) \cdot \cos(m \cdot \cos(\omega_{RF} t)) - \sin(b) \\ &\quad \cdot \sin(m \cdot \cos(\omega_{RF} t))] \end{aligned} \quad (\text{Eq. 4-12})$$

where $b \triangleq \frac{V_{bias}}{2V_{\pi}} \cdot \pi$ is a constant phase shift that is induced by the DC biased

voltage, and $m \triangleq \frac{V_m}{2V_{\pi}} \cdot \pi$ is the phase modulation index.

$$\cos(x \cdot \sin(\theta)) = J_0(x) + 2 \sum_{n=1}^{\infty} J_{2n}(x) \cos(2n\theta)$$

$$\sin(x \cdot \sin(\theta)) = 2 \sum_{n=1}^{\infty} J_{2n-1}(x) \sin((2n-1)\theta)$$

$$\cos(x \cdot \cos(\theta)) = J_0(x) + 2 \sum_{n=1}^{\infty} (-1)^n J_{2n}(x) \cos(2n\theta)$$

$$\sin(x \cdot \cos(\theta)) = 2 \sum_{n=1}^{\infty} (-1)^n J_{2n-1}(x) \sin((2n-1)\theta)$$

(Eq. 4-13, 14, 15, 16)

Expand Equation 4-12 by Bessel functions, as detailed in Equation 4-13, 14, 15 and 16. The electrical field at the output of the MZM can be written as

$$\begin{aligned} E_{out} = E_0 \cdot \cos(\omega_0 t) \cdot \\ \{ \cos(b) \cdot [J_0(m) + 2 \sum_{n=1}^{\infty} (-1)^n J_{2n}(m) \cos(2n\omega_{RF}t)] \\ - \sin(b) \cdot [2 \sum_{n=1}^{\infty} (-1)^n J_{2n-1}(m) \cos((2n-1)\omega_{RF}t)] \} \end{aligned}$$

(Eq. 4-17)

where J_n is the Bessel function of the first kind of order n. the electrical field of the mm-wave signal can be written as

$$\begin{aligned} E_{out} = E_0 \cdot \cos(b) \cdot J_0(m) \cdot \cos(\omega_0 t) \\ + E_0 \cdot \cos(b) \cdot \sum_{n=1}^{\infty} J_{2n}(m) \cdot \cos((\omega_0 - 2n\omega_{RF})t + n\pi) \end{aligned}$$

$$\begin{aligned}
& +E_0 \cdot \cos(b) \cdot \sum_{n=1}^{\infty} J_{2n}(m) \cdot \cos((\omega_0 + 2n\omega_{RF})t + n\pi) \\
& -E_0 \cdot \sin(b) \cdot \sum_{n=1}^{\infty} J_{2n-1}(m) \cdot \cos((\omega_0 - (2n-1)\omega_{RF})t + n\pi) \\
& -E_0 \cdot \sin(b) \cdot \sum_{n=1}^{\infty} J_{2n-1}(m) \cdot \cos((\omega_0 + (2n-1)\omega_{RF})t + n\pi)
\end{aligned}$$

(Eq. 4-18)

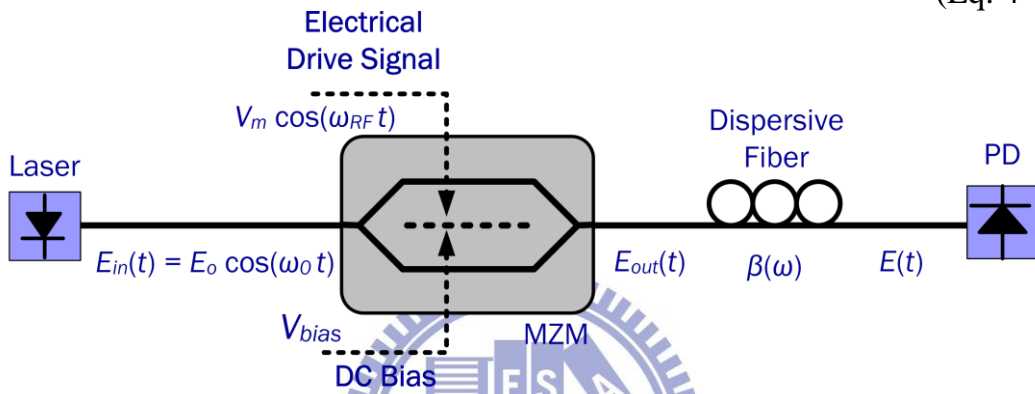


Figure 4-1 Single-electrode Mach-Zehnder Modulator.

4.2 Theoretical calculation of single drive MZM

4.2.1 Bias at maximum transmission point

When the MZM is biased at the maximum transmission point, the bias voltage is set at $V_{bias} = 0$, and $\cos(b) = 1$ and $\sin(b) = 1$. Consequently, the electrical field of the mm-wave signal can be written as

$$\begin{aligned}
E_{out} &= E_0 \cdot \cos(b) \cdot J_0(m) \cdot \cos(\omega_0 t) \\
& +E_0 \cdot \cos(b) \cdot \sum_{n=1}^{\infty} J_{2n}(m) \cdot \cos((\omega_0 - 2n\omega_{RF})t + n\pi) \\
& +E_0 \cdot \cos(b) \cdot \sum_{n=1}^{\infty} J_{2n}(m) \cdot \cos((\omega_0 + 2n\omega_{RF})t + n\pi)
\end{aligned}$$

(Eq. 4-19)

The amplitudes of the generated optical sidebands are proportional to those of the corresponding Bessel functions associated with the phase modulation index m . With the amplitude of the electrical driving signal V_m equal to V_π , the maximum m is $\frac{\pi}{2}$. As $0 < m < \frac{\pi}{2}$, the Bessel function J_n for $n \geq 1$ decreases and increases with the order of Bessel function and m , respectively, as shown in Figure 4-2. $J_1(\frac{\pi}{2})$, $J_2(\frac{\pi}{2})$, $J_3(\frac{\pi}{2})$ and $J_4(\frac{\pi}{2})$ are 0.5668, 0.2497, 0.069, and 0.014, respectively. Therefore, the optical sidebands with the Bessel function higher than $J_3(m)$ can be ignored, and Eq. 4-17 can be further simplified to

$$\begin{aligned}
 E_{\text{out}} = & E_0 \cdot \cos(b) \cdot J_0(m) \cdot \cos(\omega_0 t) \\
 & + E_0 \cdot J_2(m) \cdot \cos((\omega_0 - 2\omega_{RF})t + \pi) \\
 & + E_0 \cdot J_2(m) \cdot \cos((\omega_0 + 2\omega_{RF})t + \pi) \\
 & + E_0 \cdot J_4(m) \cdot \cos((\omega_0 - 4\omega_{RF})t) \\
 & + E_0 \cdot J_4(m) \cdot \cos((\omega_0 + 4\omega_{RF})t)
 \end{aligned}$$

(Eq. 4-20)

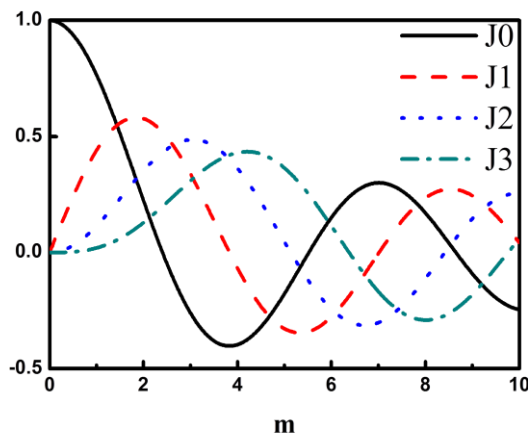


Figure 4-2 the different order of Bessel function versus m .

4.2.2 Bias at quadrature point

When the MZM is biased at the quadrature point, the bias voltage is set at $V_{bias} = \frac{V_{\pi}}{2}$, and $\cos(b) = \frac{\sqrt{2}}{2}$ and $\sin(b) = \frac{\sqrt{2}}{2}$. Consequently, the electrical field of the mm-wave signal can be written as

$$\begin{aligned}
 E_{out} = & \frac{1}{\sqrt{2}} E_0 \cdot J_0(m) \cdot \cos(\omega_0 t) \\
 & + \frac{1}{\sqrt{2}} E_0 \cdot J_1(m) \cdot \cos((\omega_0 - \omega_{RF})t) \\
 & + \frac{1}{\sqrt{2}} E_0 \cdot J_1(m) \cdot \cos((\omega_0 + \omega_{RF})t) \\
 & + \frac{1}{\sqrt{2}} E_0 \cdot J_2(m) \cdot \cos((\omega_0 - 2\omega_{RF})t + \pi) \\
 & + \frac{1}{\sqrt{2}} E_0 \cdot J_2(m) \cdot \cos((\omega_0 + 2\omega_{RF})t + \pi) \\
 & + \frac{1}{\sqrt{2}} E_0 \cdot J_3(m) \cdot \cos((\omega_0 - 3\omega_{RF})t + \pi) \\
 & + \frac{1}{\sqrt{2}} E_0 \cdot J_3(m) \cdot \cos((\omega_0 + 3\omega_{RF})t + \pi)
 \end{aligned}$$

(Eq. 4-21)

4.2.3 Bias at null point

When the MZM is biased at the null point, the bias voltage is set at $V_{bias} = V_{\pi}$, and $\cos(b) = 0$ and $\sin(b) = 1$. Consequently, the electrical field of the mm-wave signal using DSBCS modulation can be written as

$$\begin{aligned}
 E_{out} = & E_0 \cdot J_1(m) \cdot \cos((\omega_0 - \omega_{RF})t) \\
 & + E_0 \cdot J_1(m) \cdot \cos((\omega_0 + \omega_{RF})t) \\
 & + E_0 \cdot J_3(m) \cdot \cos((\omega_0 - 3\omega_{RF})t + \pi) \\
 & + E_0 \cdot J_3(m) \cdot \cos((\omega_0 + 3\omega_{RF})t + \pi) \\
 & + E_0 \cdot J_5(m) \cdot \cos((\omega_0 - 5\omega_{RF})t) \\
 & + E_0 \cdot J_5(m) \cdot \cos((\omega_0 + 5\omega_{RF})t)
 \end{aligned}$$

(Eq. 4-22)

4.3 The concept of the proposed system

Figure 4-3 depicts the concept of the proposed system [12]. The single-electrode MZM driving signal consists of an SC signal at frequency f_1 and a sinusoidal signal at frequency f_2 . In order to achieve the double sideband (DSB) with carrier suppression modulation scheme, the MZM is biased at null point. The output optical field of the MZM has two upper wavelength sidebands (USB1, USB2) and two lower wavelength sidebands (LSB1, LSB2) with carrier suppression, as shown at figure 4-2 (insect iv). After the square-law photo detection, the generated photocurrent is expressed as

$$I_{photo} = (USB1 + USB2 + LSB1 + LSB2)^2. \quad (\text{Eq. 4-23})$$

Expanding the equation 4-23 obtains the following product terms:

$$\text{Baseband} = USB1^2 + USB2^2 + LSB1^2 + LSB2^2 \quad (\text{Eq. 4-24})$$

$$\text{SC signal at frequency } f_1 + f_2 = USB1 \cdot LSB2 + USB2 \cdot LSB1 \quad (\text{Eq. 4-25})$$

$$\text{SC signal at frequency } f_2 - f_1 = USB1 \cdot USB2 + LSB1 \cdot LSB2 \quad (\text{Eq. 4-26})$$

$$\text{Beat noise} = USB1 \cdot LSB1 + USB2 \cdot LSB2 \quad (\text{Eq. 4-27})$$

The beating terms of $USB1 \cdot LSB2$ and $USB2 \cdot LSB1$ generate the desired SC-modulated electrical signals at the sum frequency. The beating terms of $USB1 \cdot USB2$, $LSB1 \cdot LSB2$, baseband and beat noise are well below the desired mm-wave frequency band and are filtered off prior to wireless transmission.

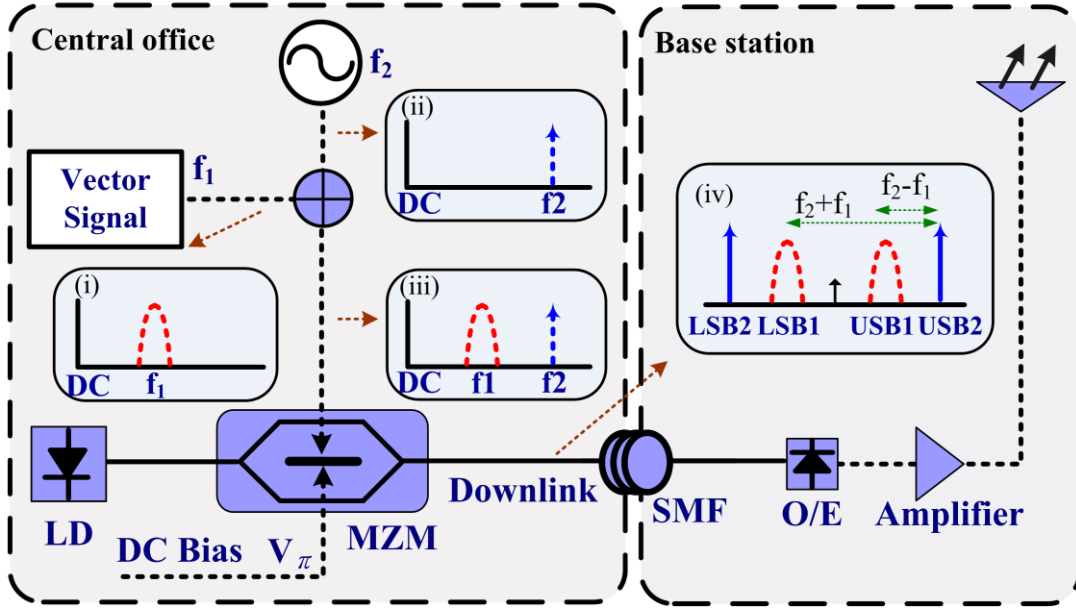


Figure 4-3 the concept of the proposed system.

4.4 Theoretical calculation of the proposed system

In this section, the theoretical equation of the proposed system is presented. Figure 4-3 shows the concept of 60 GHz RoF signal generation by one single-electrode MZM. The input optical field at the single-electrode MZM is expressed as

$$E_{in}(t) = E_0 \cdot \cos(\omega_0 t), \quad (\text{Eq. 4-28})$$

where E_0 and ω_0 are the amplitude and angular frequency of the optical source, respectively. The driving RF signal $V_{RF}(t)$ composed of two sinusoidal signals at different frequency is given by

$$V_{RF}(t) = V_1 \cos(\omega_1 t) + V_2 \cos(\omega_2 t), \quad (\text{Eq. 4-29})$$

where $V_1 \cos(\omega_1 t)$ represents that the sinusoidal signal has amplitude V_1 at frequency ω_1 and $V_2 \cos(\omega_2 t)$ is the sinusoidal signal has amplitude V_2 at frequency ω_2 . To simplify the analysis, we assume the power splitting ratio of

the MZM is 0.5. The single-electrode MZM is biased at null point for suppressing the undesired optical carrier. The output optical field of the single-electrode MZM is written as

$$E_{out}(t) = E_0 \cdot \cos(\omega_0 t) \cdot \cos\left[\left(\frac{V_\pi}{2V_\pi}\right)(V_\pi + V_1 \cos(\omega_1 t) + V_2 \cos(\omega_2 t))\right]. \quad (\text{Eq. 4-30})$$

Using Bessel function expands the equation 4-30, the output optical field is rewritten as

$$\begin{aligned} E_{out}(t) = E_0 \cdot \{ & J_0(m_2)J_1(m_1)\cos[(\omega_0 \pm \omega_1)t] \\ & - J_0(m_2)J_3(m_1)\cos[(\omega_0 \pm 3\omega_1)t] \\ & - J_1(m_1)J_2(m_2)\cos[(\omega_0 + \omega_1 \pm 2\omega_2)t] \\ & - J_1(m_1)J_2(m_2)\cos[(\omega_0 - \omega_1 \pm 2\omega_2)t] \\ & + J_0(m_1)J_1(m_2)\cos[(\omega_0 \pm \omega_2)t] \\ & - J_0(m_1)J_3(m_2)\cos[(\omega_0 \pm 3\omega_2)t] \\ & - J_1(m_2)J_2(m_1)\cos[(\omega_0 + \omega_2 \pm 2\omega_1)t] \\ & - J_1(m_2)J_2(m_1)\cos[(\omega_0 - \omega_2 \pm 2\omega_1)t] + \dots \} \end{aligned} \quad (\text{Eq. 4-31})$$

Where m_1 and m_2 are the modulation indexes defined as

$$m_i = \frac{V_i \pi}{2V_\pi} \quad i = 1, 2. \quad (\text{Eq. 4-32})$$

$J_n()$ is the n -th order Bessel function of the first kind. For a small modulation index, and the magnitude of Bessel function of the first kind is proportional to the order of the function. As shown in Figure 4-4, when modulation index is small, the output optical field can be simplified to

$$E_{out}(t) = E_0 \cdot \{J_0(m_2)J_1(m_1)\cos[(\omega_0 \pm \omega_1)t] \\ + J_0(m_1)J_1(m_2)\cos[(\omega_0 \pm \omega_2)t]\}.$$

(Eq. 4-33)

After square-law photo detection, the photocurrent of the mm-wave at frequency of $\omega_1 + \omega_2$ can be express as

$$i = R \cdot E_0 \cdot J_0(m_1)J_0(m_2)J_1(m_1)J_1(m_2)$$

where R is the responsivity of photodiode.

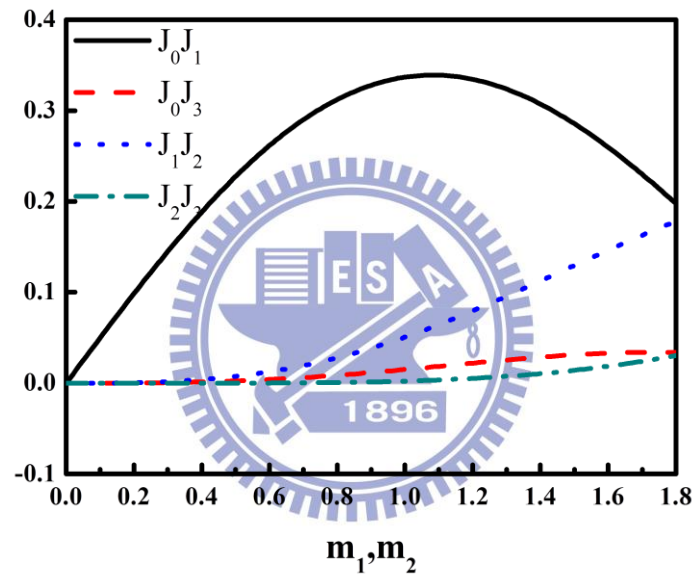


Figure 4-4

Magnitude of Bessel functions versus different modulation index.

Chapter 5

Experimental Demonstration of The Proposed System

5.1 Preface

In the previous chapter, we have introduced MIMO, FDE, and theoretical and numerical result for the proposed system. The core idea of this thesis is to integrate all these techniques significantly improving the data-rate. In this chapter, we will practically demonstrate the 60 GHz RoF system with 2x2 MIMO technology modulated with SC signal.

5.2 Experiment Setup

Figure 5-1 schematically depicts the experimental setup of the proposed 60-GHz RoF system employing 2x2 MIMO system. A simple optical transmitter using only one single-electrode MZM is utilized. To realize optical direct-detection vector signals, the driving RF signal consists of the vector signal at 22GHz and the sinusoidal signal at 38.5GHz. The single-electrode MZM is biased at the null point to suppress the undesired optical carrier. Hence, the generated optical signal consists of two data-modulated sidebands and two pilot tones as shown in Figure 5-1(a) and Figure 5-2(a). To overcome fading issue, 33/66 optical interleaver is utilized to remove one data-modulated sideband and one pilot tone as shown in Figure 5-1(b) and Figure 5-2(b).

The vector signals are generated by an arbitrary waveform generator (AWG) using a Matlab® program and up-converted to 22 GHz. One block of data comprises M ($M = 64, 128, 256, 512$) symbols of vector signals and L ($L = 4, 8, 16, 32 \dots$) symbols of CP length. 16-QAM signal with a symbol rate of 7Gbaud is utilized. Therefore, an optical SC 16-QAM signal that occupies a total bandwidth of 7 GHz can be achieved. After square-law PD detection, an electrical SC 16-QAM signal with 7GHz bandwidth is generated. The second optical signal is transmitted a further 1.5km before detection, resulting in the generation of a second uncorrelated SC 16-QAM signal. Consequently, these two independent data streams are transmitted simultaneously to realize a 2x2 MIMO wireless system. The wireless transmission distance was 3m. In practice, two independent RoF signals could be simultaneously transmitted over the same fiber by using the polarization-division-multiplexing (PMD) or wavelength-division-multiplexing (WDM) schemes. Two pairs of the mixed signals at 60.5 GHz were down-converted to 5.5 GHz as shown in inset (c) of Figure 5-1 and Figure 5-3 and captured by a real time scope with a 50-GHz sample rate and a 3-dB bandwidth of 12.5 GHz. An off-line DSP program was employed to demodulate the MIMO signals. The overhead of the signal is $L / (M+L)$, and the total data rate with 2x2 MIMO technology is $4 \times 2 \times [M / (M+L)]$ Gb/s. The MIMO demodulation process includes synchronization, FDE, zero-forcing algorithm, and QAM symbol decoding. The bit error rate (BER) performance is calculated from the measured error vector magnitude (EVM).

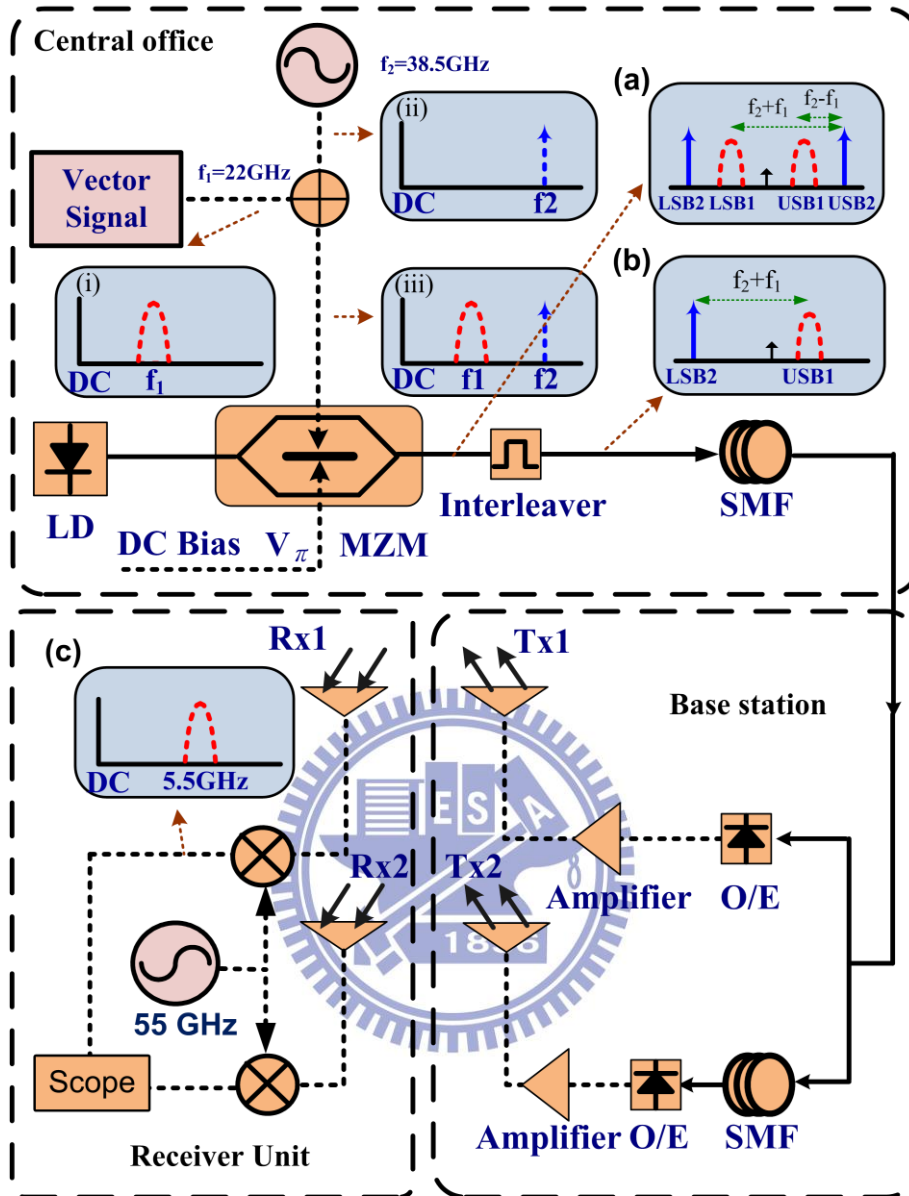


Figure 5-1 experimental setup of the propose system.

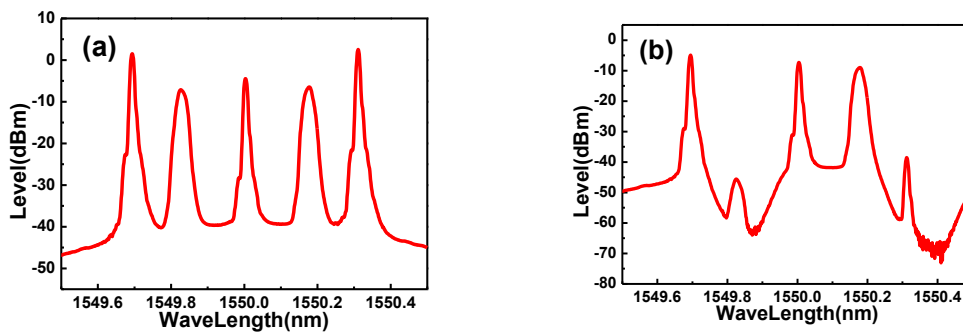


Figure 5-2 optical spectrum for 16 QAM SC signal.

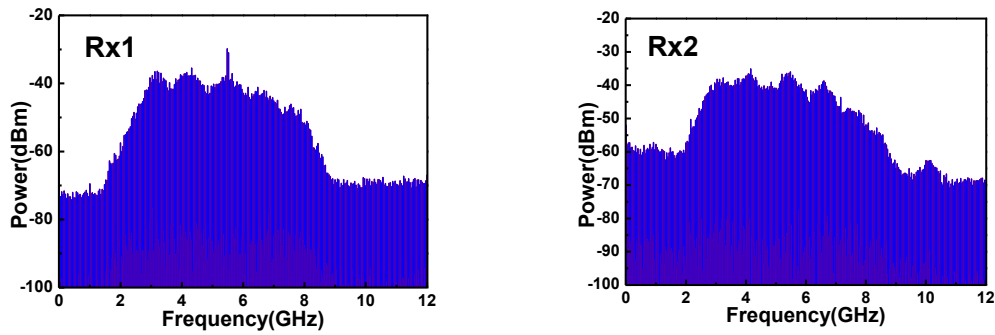


Figure 5-3 electrical spectrum for 16 QAM SC signal.

5.3 Experimental Result for SC Signal with SISO Channel

SISO channel means only one transmit antenna and one receive antenna are used in this system. We consider the effect of uneven frequency response caused by the response of components and in-band distortion induced by fiber dispersion. Frequency domain equalizer at receiver compensates the frequency-selective channel and recovers the distortion signal suffering from serious ISI. In this section, we will show the experiment result of QPSK, 8-QAM and 16-QAM SC carrier signals with SISO channel employed the FDE at receiver.

5.3.1 Transmission Result of SC QPSK Signal (SISO)

To implement FDE at receiver, the transmitted signal should be arranged to the block form. Every 256 data symbols consist a block and the CP length is the last 8 symbols of the 256 data symbols. Figure 5-4 illustrates the BER curve of SC QPSK signal in back to back (BTB) and after transmission over 25-km single mode fiber (SMF). Data rate achieve 6.79 Gb/s and the power penalty after transmission over 25-km single-mode fiber is negligible.

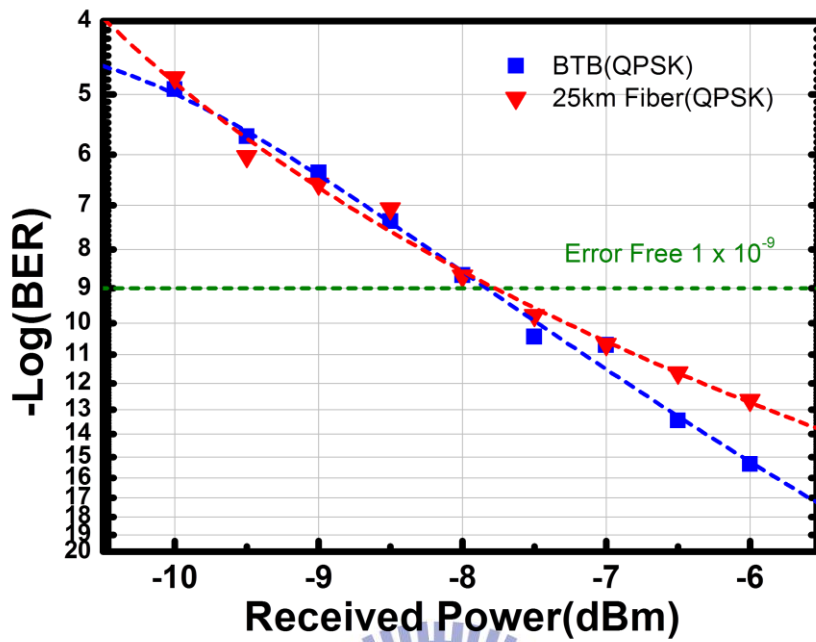


Figure 5-4 BER curve of QPSK SC signal with SISO channel.

Figure 5-5 shows QPSK constellation diagrams in BTB and 25 km SMF transmission. Photodiode (PD) received power is -6dBm. The BER has been much lower than error-free limit 1×10^{-9} .

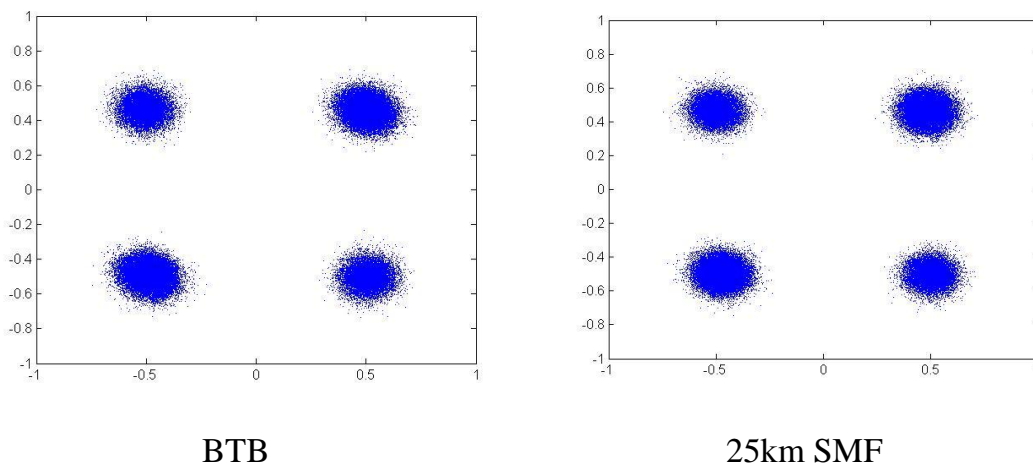


Figure 5-5 Constellations of the QPSK SC signal with SISO channel

5.3.2 Transmission Result of SC 8-QAM Signal (SISO)

Figure 5-6 shows the transmission result of the SC 8-QAM signal using FDE at receiver to compensate the uneven frequency response. Every block length is 256 data symbols, and the CP length is 8 symbols. The BER curve of SC 8-QAM signal in BTB and after transmission over 25-km SMF only have slight difference, so the power penalty can be negligible. Data rate 10.18 Gb/s is obtained in this scenario.

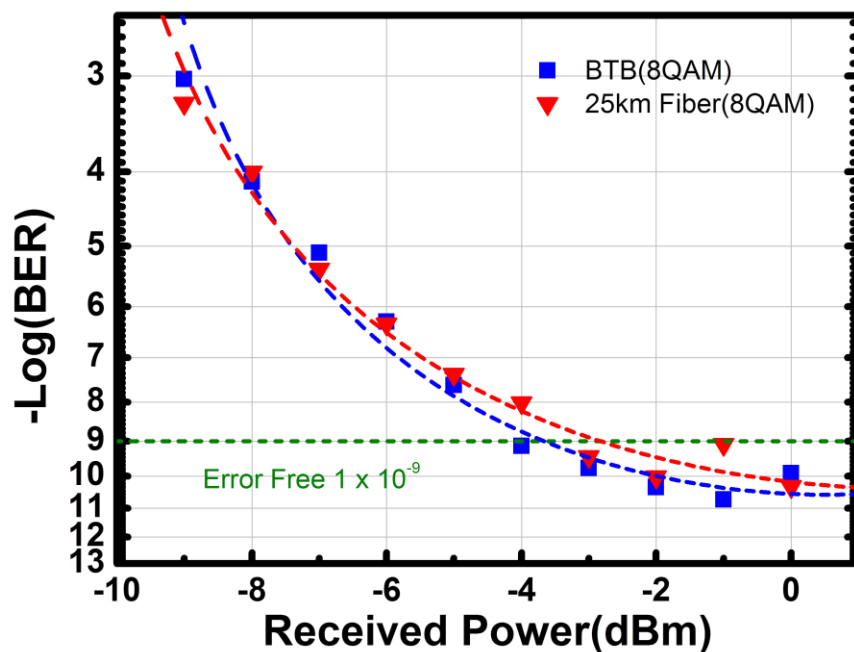


Figure 5-6 BER curve of 8-QAM SC signal with SISO channel.

The constellation diagram of SC 8-QAM signal in BTB and 25km SMF transmission are shown in figure 5-7. PD received power is -2dBm at the saturated point.

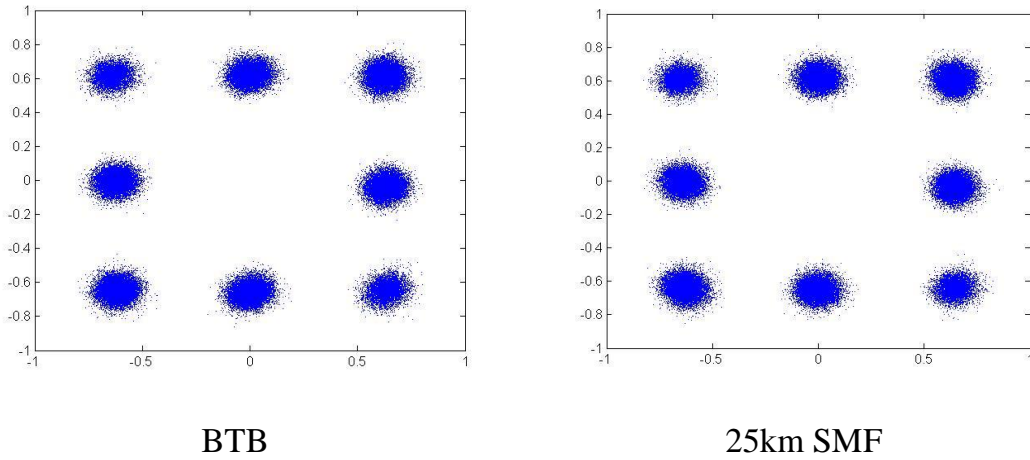


Figure 5-7 Constellations of the 8-QAM SC signal with SISO channel.

5.3.3 Transmission Result of SC 16-QAM Signal (SISO)

SC 16-QAM signal is decoded by FDE. FFT size is 256 data symbols, and CP length is 8. Figure 5-8 illustrates the BER curve of SC 16-QAM signal in BTB and after transmission over 25-km SMF. Both in BTB and after 25km SMF situation, the BER can lower than the newly FEC limit 3.8×10^{-3} . Thus, the data rate achieves 13.58 Gb/s and the sensitivity penalty is negligible.

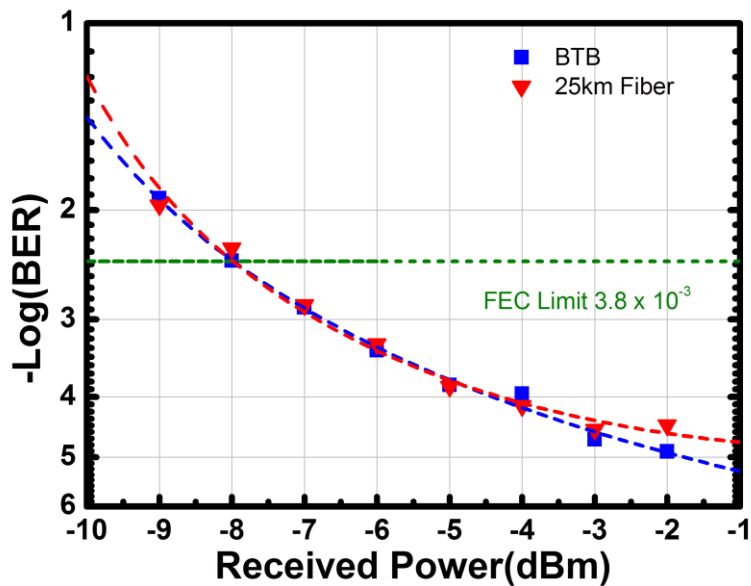


Figure 5-8 BER curve of 16-QAM SC signal with SISO channel.

Figure 5-9 shows the constellation diagrams of 16QAM signal after system in BTB and after 25 km SMF transmission. They are captured at PD received power equal to -2dBm.

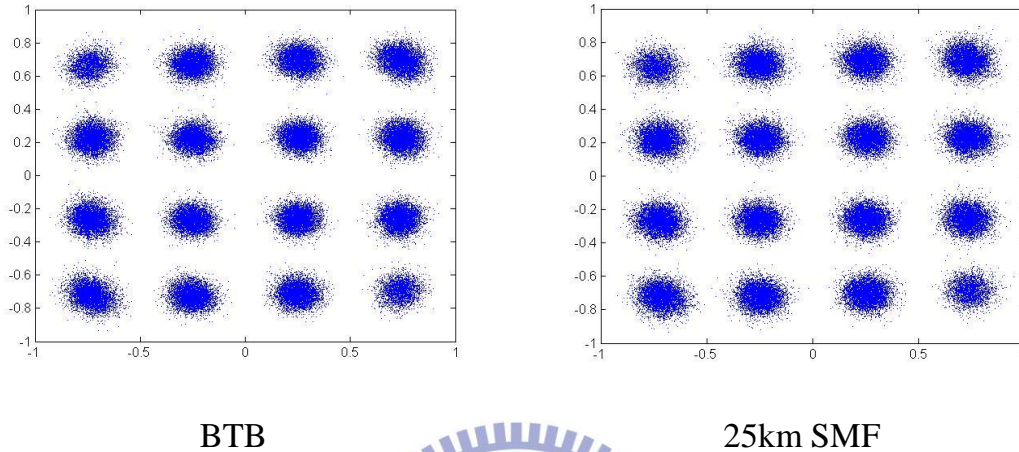


Figure 5-9 Constellations of the 8-QAM SC signal with SISO channel.

5.4 Experimental Result for SC Signal with MIMO Technology

In this section, we find the optimal condition of FDE for the proposed system at first. There are two main parameters in FDE. One is the number of data symbols in one block and the other is CP length in one block. We also analyze the effect of the channel correlation over MIMO channel. At last, the transmission result of 60GHz RoF system with MIMO technology is shown.

5.4.1 SC MIMO signal at different FFT size of FDE

The number of data symbols in one block is related to the number of points of FFT, and the resolution in frequency is better and better with increasing the FFT size. However, the short FFT size has poor performance, and the long FFT size has higher complexity of computation. In order to

combat the uneven frequency response, we find an appropriate FFT size for the propose system.

Figure 5-10 shows the experiment result with different FFT sizes of FDE MIMO 16-QAM signals in BTB transmission. The CP length is fixed to 8 symbols which have same ability to avoid IBI, and the FFT size is 64, 128, 256, 512 symbols per block. More symbols in one data block represent that the resolution in the frequency domain would be higher form FFT size 64 to FFT size 512. Thus, FFT size 128 is better than FFT size 64, and FFT size 256 is better than FFT size 128 for the performance of the signals after FDE. Notice that the performance of FFT 512 only gets slight improvement from FFT size 256. In the other word, FFT size 256 is enough to resist ISI in the proposed system.

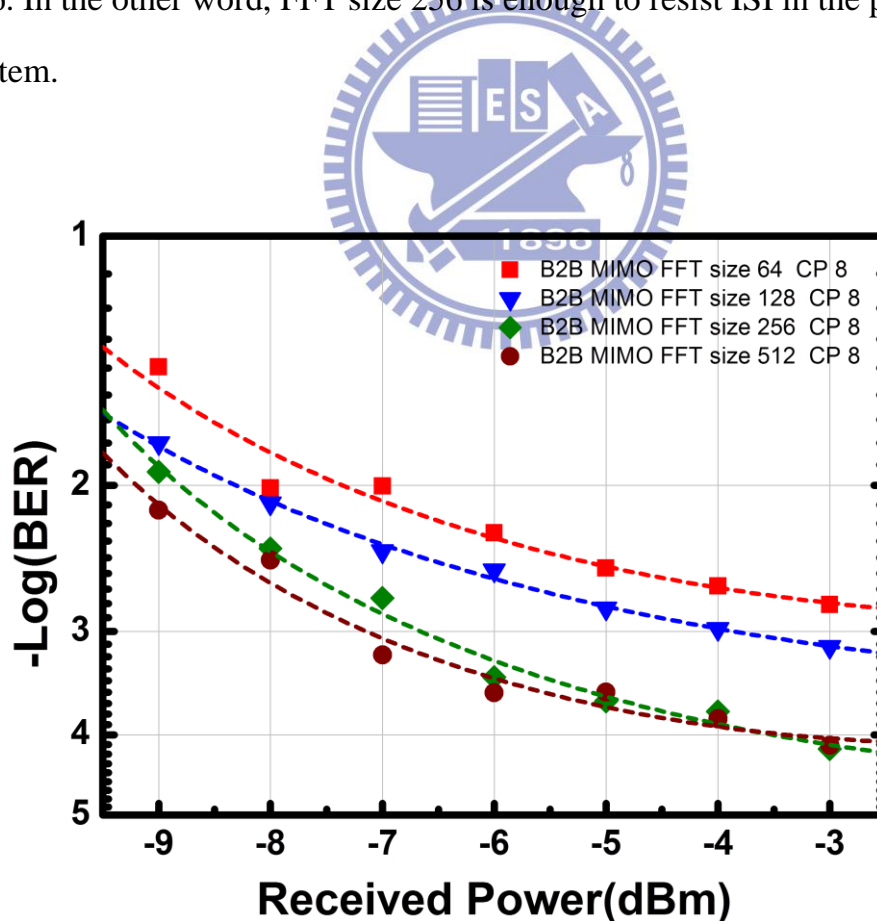


Figure 5-10 BER curve of 16-QAM SC signal with MIMO channel in BTB transmission at different FFT size.

5.4.2 SC MIMO signal at different CP length of FDE

CP length is important in the proposed MIMO system. It not only can resist the inter-block interference (IBI) but also can improve the tolerance to the signal delay caused by LOS MIMO channel in the air. Thus, the suitable CP length will be found in order to have enough ability resisting IBI and not to increase too much overhead of the data.

Figure 5-11 shows the BER curve of the 16QAM MIMO signal with different CP length. The FFT size is 256, and the CP length is 4, 8, 16, 32 symbols. When CP length is 4 symbols, the overhead is only 4/260 which is the smallest of these four conditions. However, if the CP length is so short that couldn't resist the inter-block interference, the performance would decrease because of the imperfect circular convolution. As the figure 5-11 is shown, when the CP length is more than 8 symbols, the IBI could be neglected.

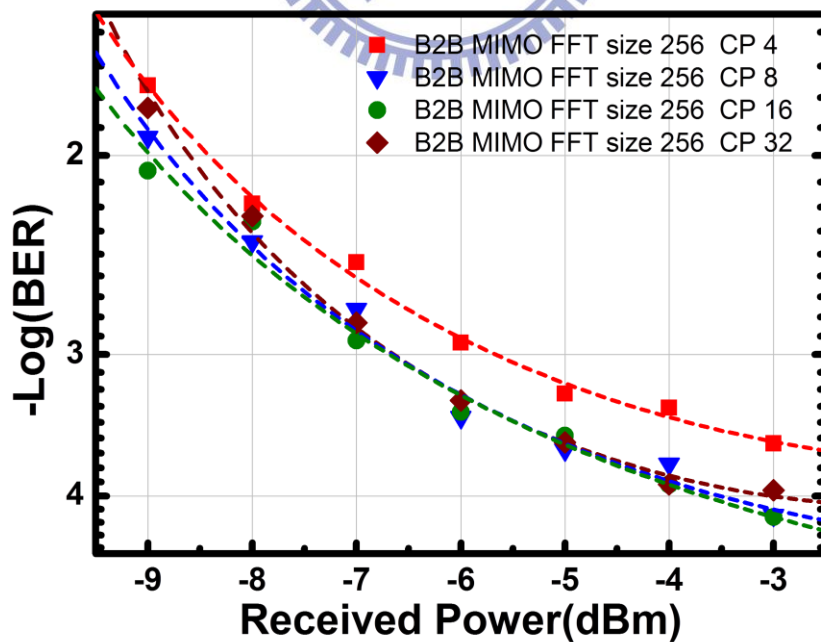


Figure 5-11 BER curve of 16-QAM SC signal with MIMO channel in BTB transmission at different CP length.

5.4.3 SC MIMO Signal at Different Channel Correlation

The higher channel correlation will result in noise enhancement in the MIMO scenario, and we have to know how much the penalty the system has because of channel correlation. Figure 5-12 indicates the relation between channel correlation and signal to noise ratio (SNR). The transmission is SC 16-QAM signal with FFT size 256 and 8 CPs. We change the MIMO channel correlation by adjusting the antenna spacing. We can see that the performances of the SISO channel from one transmit antenna to the two receive antennas which are SISO_ch1 and SISO_ch2 respectively is the same no matter what MIMO channel correlation it is. The performance doesn't decay at different antenna spacing with the SISO channel. However, in the MIMO scenario, the performance will decrease faster and faster with the ascent of the channel correlation. At the best condition of this experiment, the penalty is about 0.5 dB between SISO and MIMO.

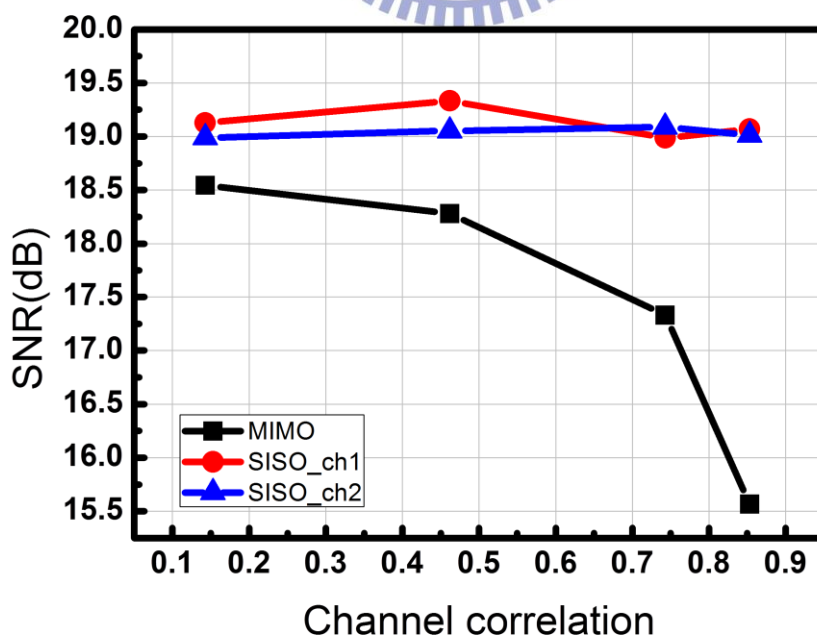


Figure 5-12 SNR versus MIMO Channel correlation of 16-QAM SC signal in BTB transmission.

5.4.4 Transmission Result of SC QPSK Signal (MIMO)

Figure 5-13 illustrates the BER curve of QPSK SC MIMO signal in BTB and after 25km SMF transmission. The FFT size and CP length of FDE are in the optimal condition as mentioned before. Every 256 data symbols form a block and CP length is 8 symbols. Data rate is 13.58 Gb/s in this system. The power penalty between BTB and 25 km SMF transmission is about 0.2dB which is small enough to ignore.

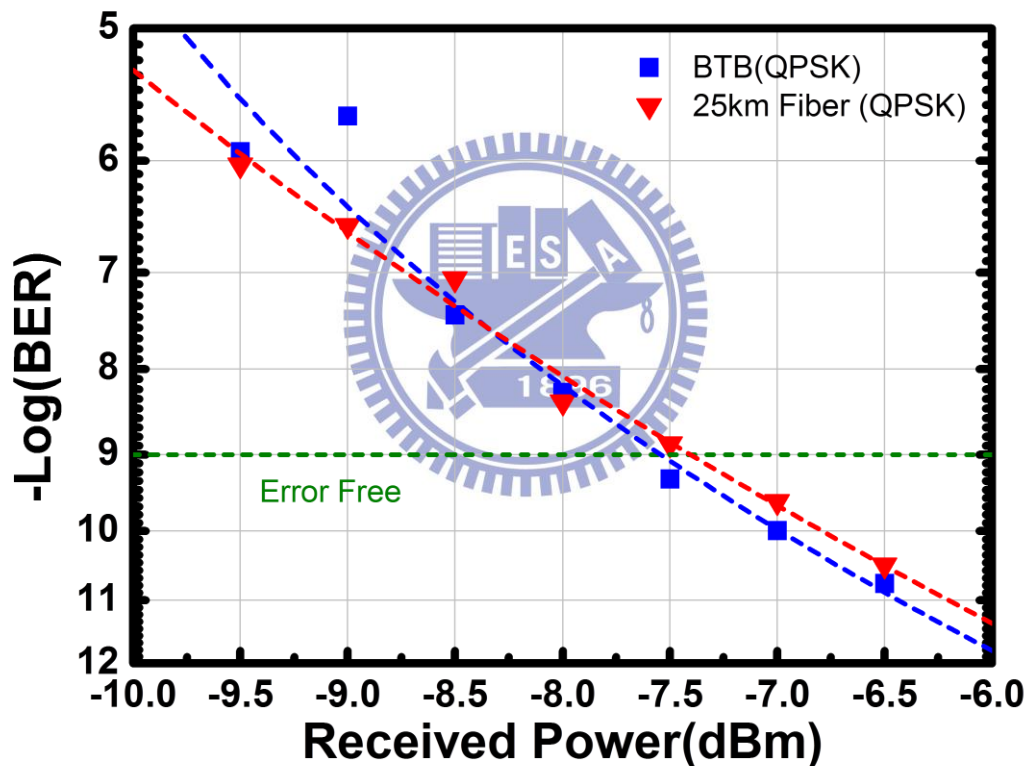


Figure 5-13 BER curve of QPSK SC signal with MIMO channel.

Figure 5-14 shows QPSK constellation diagrams for the Tx1, Tx2 and Tx1+Tx2 MIMO transmission in back-to-back (BTB) and following single-mode fiber transmission cases. The PD received power is -6.5dBm.

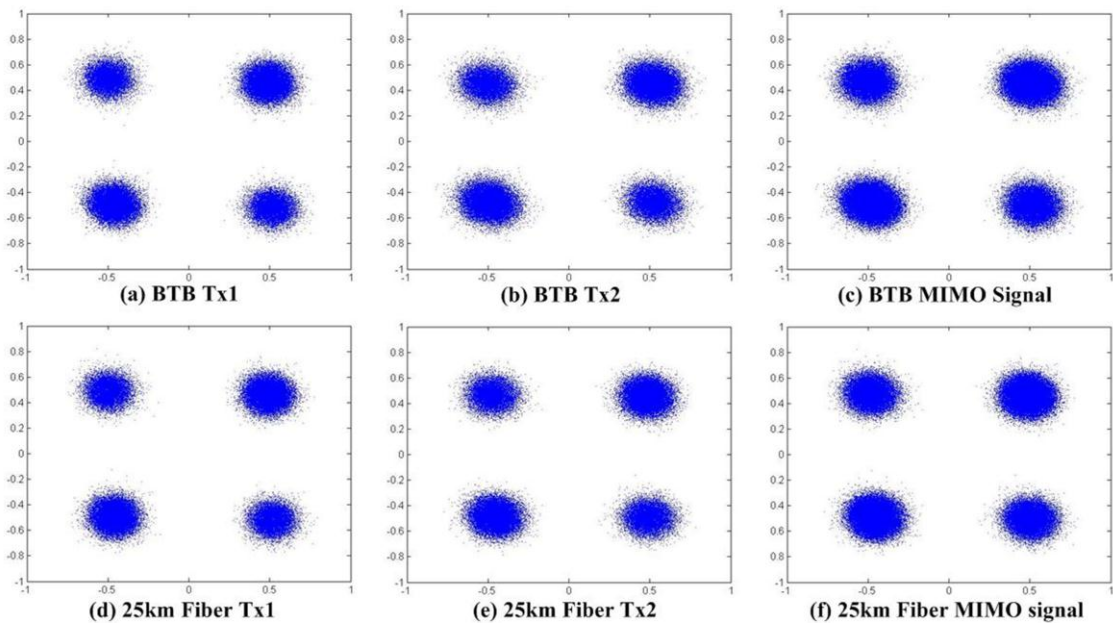


Figure 5-14 Constellations of the QPSK MIMO signal.

5.4.5 Transmission Result of SC 8-QAM Signal (MIMO)

SC signal modulated 8-QAM with 7 GHz bandwidth in the MIMO scenario can achieve data rate up to 21 Gb/s, but the overhead come from CP should be considered. FFT size of FDE is 256 data symbols and CP length is 8 symbols. Thus, the overall data actually is 20.36 Gb/s. Figure 5-15 shows that the BER curve of 8-QAM SC MIMO signal in BTB and after 25km SMF transmission. When the PD received power is lower than -10dBm, both of the transmit conditions can obtain the FEC limit. The power penalty can ignore.

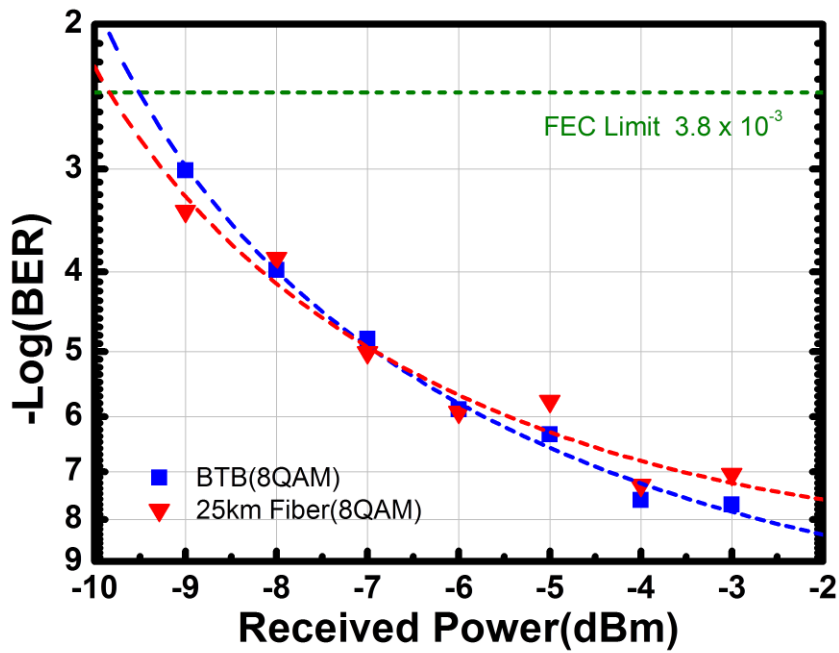


Figure 5-15 BER curve of 8-QAM SC signal with MIMO channel.

Figure 5-16 illustrates 8-QAM constellation diagrams for the Tx1, Tx2 and Tx1+Tx2 MIMO transmission after system in back-to-back (BTB) and following single-mode fiber transmission cases. The PD received power is -3dBm.

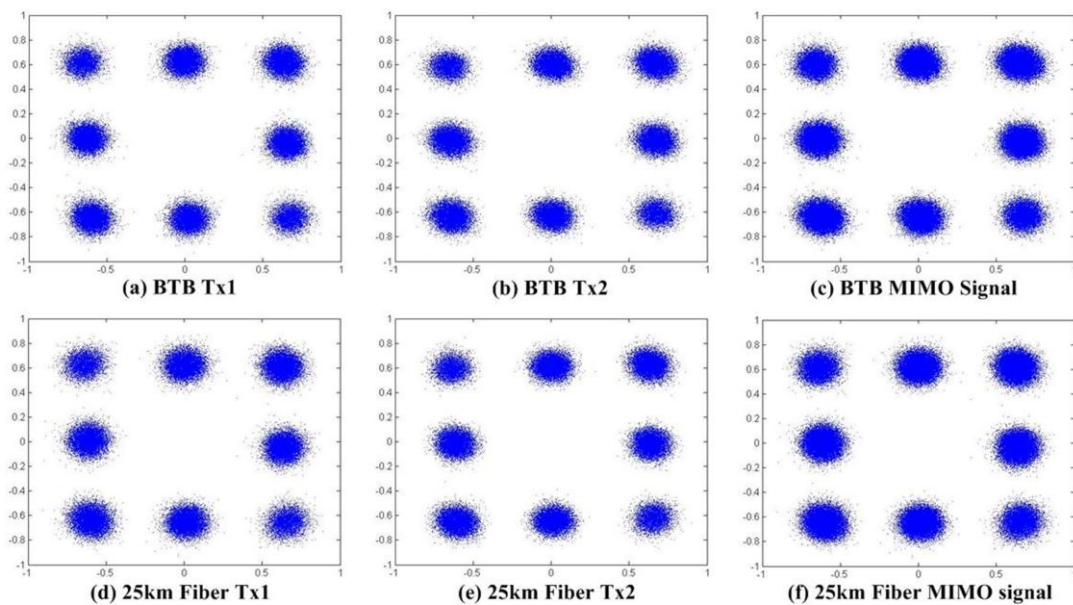


Figure 5-16 Constellations of the 8-QAM MIMO signal.

5.4.6 Transmission Result of SC 16-QAM Signal (MIMO)

Figure 5-17 indicates the BER curves of 16-QAM SC MIMO signal in BTB and after 25km SMF transmission. FFT size of FDE still is optimal value 256 data symbols, and CP length remains 8 symbols. The transmission can be error-free by FEC, and data rate achieves up to 27.15 Gb/s in the proposed system without power penalty in BTB and after 25km SMF transmission. However, the performance of the system can't support the higher order data format such as 32-QAM, 64-QAM.... Thus, 16-QAM SC MIMO signal with 7 GHz band in the proposed 60GHz RoF system obtains the highest data rate in this thesis.

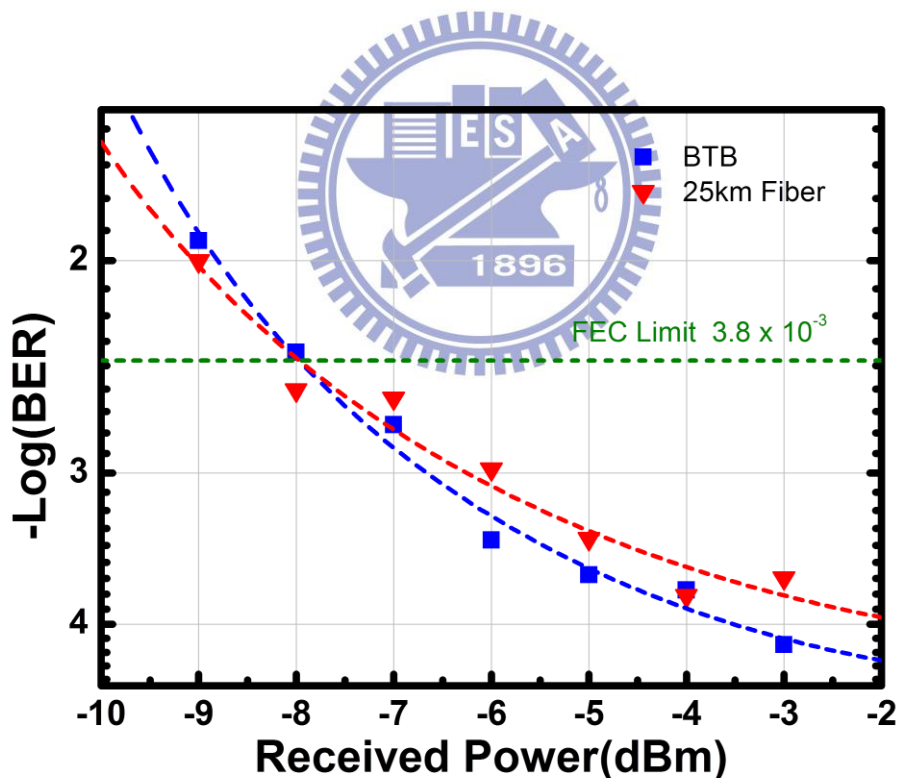


Figure 5-17 BER curve of 16-QAM SC signal with MIMO channel.

The constellation diagram of 16-QAM MIMO signal for the Tx1, Tx2 and Tx1+Tx2 MIMO transmission after system in back-to-back (BTB) and following single-mode fiber transmission cases as shown in figure 5-18. The PD received power is -3dBm.

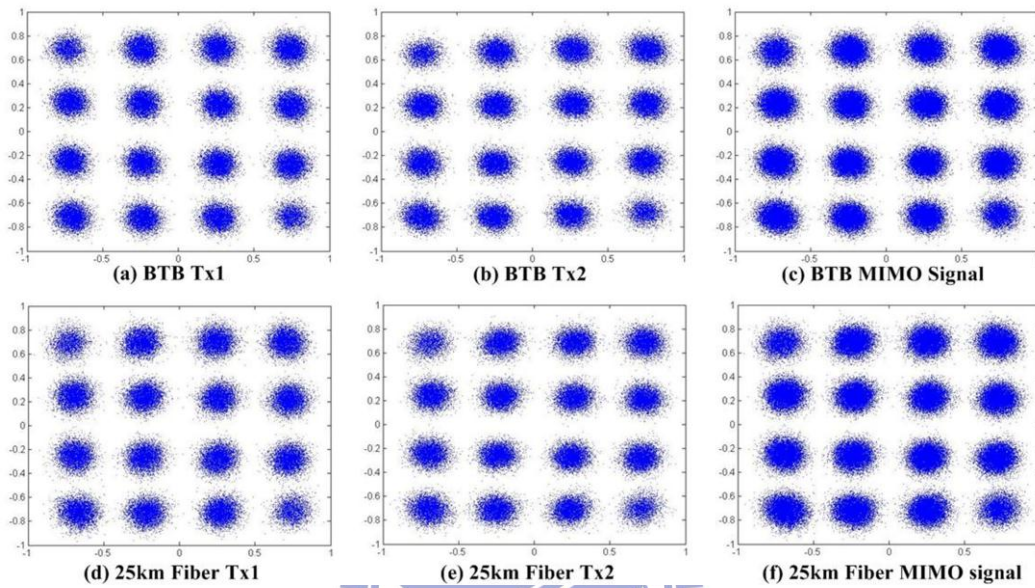
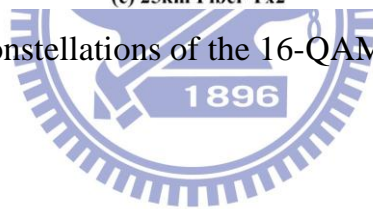


Figure 5-18 Constellations of the 16-QAM MIMO signal.



Chapter 6

Conclusion

This work demonstrates the high speed 60 GHz radio over fiber system with 2 x 2 multiple-input and multiple-output antenna technology for the improvement of spectrum efficiency. We generate the 60.5 GHz electrical RF signals by one single-electrode MZM. Then, MIMO technique is realized by two transmit antennas which transmit two independent data streams to the two receive antenna through the air channel. Frequency domain equalizer is induced to compensate non-flat channel response with up to 10dB deviation within the 7 GHz bandwidth and separate the MIMO signals by zero-forcing algorithm.

The experiment result of different data formats (QPSK, 8-QAM and 16-QAM) with SISO channel is presented at first. The optimal conditions of the FFT size and CP length in FDE for the proposed system are found. Moreover, we also show the penalty between the SISO and MIMO transmission with various MIMO channel correlation.

At last, we experimentally demonstrate the efficacy of 2 x 2 LOS MIMO techniques for wireless data capacity improvement at 60 GHz with a 27.15-Gbps wireless signal transmission using 7 GHz license-free spectrum at 60GHz and single-carrier data modulation. Transmission over 25-km standard single-mode fiber and 3m wireless distance were achieved with negligible penalty.

References

- [1] Report of the Unlicensed Devices and Experimental Licenses Working Group, Federal Communications Commission Spectrum Policy Task Force, 15th Nov 2002.
- [2] Amendment of Part 2 of the Commission's Rules to Allocate Additional Spectrum to the Inter-Satellite, Fixed, and Mobile Services and to Permit Unlicensed Devices to Use Certain Segments in the 50.2-50.4 GHz and 51.4-71.0 GHz Bands, FCC 00-442, Federal Communications Commission, Dec 2000.
- [3] R. Emrick, S. Franson, J. Holmes, B. Bosco, and S. Rockwell, "Technology for Emerging Commercial Applications at Millimeter-Wave Frequency", IEEE/ACES Int. Conf. Wireless communications and Applied Computational Electromagnetics, pp. 425-429, April 2005.
- [4] A. Ng'oma, "Radio-over-Fibre Technology for Broadband Wireless Communication Systems", 2005.
- [5] David Tse, Pramod Viswanath, Fundamental of Wireless Communication, 2005.
- [6] Tim Schenk, RF Imperfections in High-rate Wireless Systems Impact and Digital Compensation, 2008.
- [7] C. Oestges and B. Clerckx MIMO WIRELESS COMMUNICATION From Real-World Propagation to Space-Time Code Design, 2007.
- [8] Wikipedia, "Comparison of wireless data standard", http://en.wikipedia.org/wiki/Comparison_of_wireless_data_standards, 2011.
- [9] D. Falconer, S. L. Ariyavisitakul, A. Benyamin-Seeyar and B. Eidson, "Frequency Domain Equalization for Single-Carrier Broadband

Wireless Systems”, IEEE Communications Magazine, Vol. 40, pp. 58-66, Apr 2002.

- [10] Siavash M. Alamouti, “A simple transmit diversity technique for wireless communications”, IEEE Journal on Selected Areas in Communications, Vol. 16, pp. 1451-1458, Oct 1998.
- [11] A. V. Oppenheim and R. W. Schaffer, Discrete-Time Signal Processing, 2nd, pp. 571-588, 1998.
- [12] W. J. Jiang; C. T. Lin, A. Ng'oma, P. T. Shih, J. Chen, M. Sauer, F. Annunziata and S. Chi “Simple 14-Gb/s Short-Range Radio-Over-Fiber System Employing a Single-Electrode MZM for 60-GHz Wireless Applications” , Journal of Lightwave Technology, Vol. 28, pp. 2238-2246, Aug 2010.

